ELSEVIER

Biochimica et Biophysica Acta 1565 (2002) 267–286

BIOCHIMICA ET BIOPHYSICA ACTA
BBA

www.bba-direct.com

Review

Recent advances in ion channel research ☆

Shin-Ho Chung [a,*], Serdar Kuyucak [b]

[a] Protein Dynamics Unit, Department of Physics, Faculty of Sciences, Australian National University, Canberra, A.C.T. 0200, Australia
[b] Department of Theoretical Physics, Research School of Physical Sciences, Australian National University, Canberra, A.C.T. 0200, Australia

Received 18 February 2002; received in revised form 10 May 2002; accepted 29 May 2002

Abstract

The field of ion channels has entered into a rapid phase of development in the last few years, partly due to the breakthroughs in determination of the crystal structures of membrane proteins and advances in computer simulations of biomolecules. These advances have finally enabled the long-dreamed goal of relating function of a channel to its underlying molecular structure. Here we present simplified accounts of the competing permeation theories and then discuss their application to the potassium, gramicidin A and calcium channels.

Keywords: Membrane ion channel; Brownian dynamics; Molecular dynamics; Channel modeling; Theories of ion permeation

1. Introduction

The measurement of ionic currents flowing through single channels in cell membrane has been made possible by the giga-seal patch-clamp technique [1,2]. A tight seal between the rim of the electrode tip and the cell membrane drastically reduces the leakage current and extraneous background noise, enabling the resolution of the discrete changes in conductance, which occur when single channels open or close. The technique has so far proved to be a powerful tool for characterizing biologically important currents. Because all electrical activities in the nervous system, including communication between cells and the influence of hormones and drugs on cell function, are regulated by membrane ion channels, understanding their mechanisms at a molecular level is a fundamental problem in neurobiology. Moreover, elucidation of how single channels work will ultimately help us find the causes of, and possibly cures for, a number of neurological and muscular disorders.

Despite the wealth of information accumulated over the past two decades, some of the outstanding questions about how biological channels work remain unanswered. The first among these questions is the detailed dynamical processes underlying the permeation of ions across an open channel. An ion in electrolyte solution does not move freely but drags along a shell of water that is semipermanently bound to it. To give an example, the electrostatic binding energy of a water molecule in the first hydration shell of a sodium ion is about 10^{-19} J or 24 kT in room temperature units. This is a huge energy compared to the average kinetic energy of ions. To move across a narrow conduit, such as the selectivity filter of the potassium channel, the ion-water geometry needs to be rearranged, with partially dehydrated ions interacting electrostatically with the charged residues on the protein wall. Secondly, all biological ion channels are selectively permeable to a specific ion. Channels generally discriminate anions from cations; some channels select sodium ions but reject potassium ions or vice versa. This selectivity mechanism needs to be understood in terms of the interactions of the permeating ions with the surrounding water and protein molecules. Thirdly, what determines the upper-limit in channel conductance? To be functionally effective, a channel must process a large number of ions but, at the same time, it has to be highly selective to specific ionic species. It is a challenge to unravel the design that most satisfactorily reconciles these conflicting requirements. Fourthly, what kind of structural changes take place when a

Abbreviations: PNP, Poisson–Nernst–Planck; BD, Brownian dynamics; MD, molecular dynamics; GA, gramicidin A; PMF, potential of mean force

☆ Three video clips referred to in the text may be downloaded from: http://langevin.anu.edu.au or www.elsevier.com/PII/S00052736020005746.

* Corresponding author. Tel.: +61-2-6125-2024; fax: +61-2-6247-2792.

E-mail address: shin-ho.chung@anu.edu.au (S.-H. Chung).

0005-2736/02/$ - see front matter © 2002 Elsevier Science B.V. All rights reserved.
PII: S0005-2736(02)00574-6

channel makes transitions from the closed conformation to the open conformation? Whether the gating of biological ion channels is steric or controlled electrostatically, such as by rotating the orientations of a ring of dipoles guarding the channel gate, remains to be elucidated. Finally, the tertiary structures of all known ionic channels need to be determined. The solutions proposed for the unsolved questions have to be consistent with the channel structure deduced by protein chemists.

During the past several years, there have been enormous strides in our understanding of the structure–function relationships in biological ion channels. This sudden advance has been brought about by the combined efforts of experimental and computational biophysicists, who together are beginning to unravel the working principles of these exquisitely designed biological macromolecules that regulate the ionic gradients across the living membrane. In a recent breakthrough, the molecular structures of the *Streptomyces lividans* potassium channel, mechanosensitive channel and chloride channel have been determined from crystallographic analyses [3–5]. It is expected that crystal structures of other ion channels will follow these discoveries, ushering us into a new era in ion channel studies, where predicting the function of channels from their atomic structures will become the main quest. Parallel to these landmark experimental findings, there have been also important advances in computational biophysics. As new analytical methods have been developed and the available computational power increased, theoretical models of ion permeation have become increasingly sophisticated. Now it has become possible to relate the atomic structure of an ion channel to its function, through the fundamental laws of physics operating in electrolyte solutions. Many aspects of macroscopic observable properties of ion channels are being addressed by molecular and stochastic dynamics simulations. Intuitive and hand-waving explanations of the permeation and selectivity of ions are beginning to be replaced by quantitative statements based on rigorous physical laws.

Here we give an overview of recent advances in biophysics of ion channels, placing a special emphasis on theoretical approaches that are currently under development. Computational methods of solving complex biological problems, such as permeation, selectivity and gating mechanisms in ion channels, will increasingly play prominent roles as the speed of computers increases. Our aim in this article is to provide some understanding of various methods that have been proposed for treating time-dependent, nonequilibrium processes that underlie the flow of currents across biological ion channels. The tools of physics that are employed in this endeavor, from fundamental to phenomenological, are ab initio and classical molecular dynamics (MD), stochastic dynamics and continuum theories. In MD simulations, trajectories of all the atoms in a system are followed using Newton's equation of motion. In ab initio MD, the interaction between the atoms are determined from first principles electronic structure calculations. As there are no free parameters in this approach, it presents the ultimate approach to modeling of biomolecular systems. But because of the extremely demanding nature of computations, its applications are limited to very small systems at present. In classical MD, simulations are carried out using empirically determined pairwise interaction potentials between the atoms. While it is possible to model an entire ion channel in this way, it is not feasible to simulate the system long enough to see permeation of ions across a model channel and to determine its conductance, which is the most important channel property. For that purpose, one has to go further down to stochastic dynamics, where water molecules that form the bulk of the system in ion channels are integrated out and only the ions themselves are explicitly simulated. The continuum electrodiffusion theory of Poisson–Nernst–Planck (PNP) equations makes one further simplification known as the mean-field approximation. Here, ions are treated not as discrete entities but as continuous charge densities that represent the space-time average of the microscopic motion of ions. In PNP, the flux of an ionic species is described by the Nernst–Planck equation that combines Ohm's law with Fick's law of diffusion, and the potential at each position is determined from the solution of Poisson's equation using the total charge density (ions plus fixed charges). The PNP theory thus incorporates the channel structure and its solution yields the potential, concentration and flux of ions in the system in a self-consistent manner.

There is one other approach that has been fruitfully employed to model biological ion channels, namely, the reaction rate theory [6]. In this approach, an ion channel is represented by a series of ion binding sites separated by barriers, and ions are assumed to hop from one biding site to another, the probability of each hop determined by the height of the energy barrier. Many useful insights have been gleaned in the past about the mechanisms of ion permeation using this approach. The merits and demerits of this theory have been debated extensively in the literature [7–12] to which the interested reader is referred to. We will not discuss the rate theories further in this article because the model parameters have no direct physical relation to the channel structure whereas our focus is on the structure–function relationships.

This review article is primarily devoted to the three computational approaches—molecular dynamics, stochastic dynamics and continuum theories—to unravel the inner workings of biomolecules. We give intuitive explanations of the physics underlying each of the methods, referring mathematical details to more comprehensive publications. We discuss the merits and shortcomings of each computational approach. Detailed accounts of recent experimental findings on ion channels are not given here; the reader is referred to the latest edition of Hille [6], which provides an excellent source of information in this regard.

The paper is organized as follows. We first describe the principles underlying the continuum theories, stochastic dynamics, and molecular dynamics, stressing the strengths

and weaknesses of each approach. We then discuss briefly how these computational tools have been applied in studying selectivity and permeation of ions in biological channels. We do not attempt to give an exhaustive review of the literature, which is given elsewhere [7,8,13–18]. Instead, we discuss a few selected examples to illustrate how the theories are applied in modeling of ion channels. We conclude the paper by highlighting future directions for research and identifying the problems in different approaches that need to be resolved.

2. Theoretical tools for studying ion channels

2.1. Continuum theories

2.1.1. Ohm's and Fick's laws and Nernst–Planck equation

The flow of ions across a channel is controlled by the potential and concentration differences on the two sides of the cell membrane. The potential difference creates an electric field across the channel, which drives cations in the direction of the field and anions in the opposite direction. The relationship between the current density and the potential gradient (or the electric field) is expressed by Ohm's law

$$\mathbf{J} = -g\nabla\varphi = g\mathbf{E}, \tag{1}$$

where g is the conductivity of the electrolyte solution whose values are determined from experiments under various conditions. To make contact with the more familiar expression $I=GV$, where I is the channel current, V is the membrane potential, and G is the channel conductance, we consider a cylindrical channel with radius r and length L. Assuming a uniform current density and electric field across the channel, we have $\mathbf{J}=I/\pi r^2$ and $\mathbf{E}=V/L$. Substituting these values in Eq. (1) yields Ohm's law with the conductance given by

$$G = \pi r^2 g/L. \tag{2}$$

A similar line of analysis can be carried out for channels with more complicated geometries, such as biconical or catenary shape [19].

The physical basis of Ohm's law can be easily understood in terms of the microscopic motion of ions in water. Ions in an electrolyte solution incessantly collide with the surrounding water molecules and as a result execute a random Brownian motion with an average collision time τ. When an electric field $\mathbf{E}$ is applied, an ion with mass m and carrying a unit charge e accelerates, on average, for time τ, gaining a drift velocity, $\mathbf{v}_d=(e\mathbf{E}/m)\tau$. Ohm's law follows when this drift velocity is substituted in the definition of the current density

$$\mathbf{J} = ne\mathbf{v}_d = \frac{ne^2\tau}{m}\,\mathbf{E}, \tag{3}$$

where n is the number density of the ions, which is related to the concentration c (in mol/l) by $n=1000\,N_A c$ where N_A is Avogadro's number. Eq. (3) also provides a microscopic expression for the conductivity in terms of the properties of the ion, $g=n\,e^2\tau/m$. This simple expression works in gases but not in electrolyte solutions where the correlation of water molecules with the ions must be taken into account in order to obtain sensible results. This can be done most simply using the solvent model where the hydration waters are considered as permanent fixtures around the ion. As a result, the ion acquires an effective mass and radius, which are significantly larger than their bare values. Using the fact that the average collision time τ is the mean free path divided by the average speed, one can derive a phenomenological expression for the conductivity in terms of the effective mass and radius of the ion [19].

Ohm's law, simple as it may be, can provide us with useful insights about the permeation mechanisms across a transmembrane pore. As an example, we consider the gramicidin A channel, a cylindrical pore whose radius r and length L are approximately 2 and 25 Å, respectively. The experimentally determined conductivity of 150 mM K^+ ions is $g=8.4\times10^{-3}$ S/cm in the conventional units of Siemens (S) for conductance. Substituting these values in Eq. (2), we obtain $G=42$ pS. For an applied potential of 200 mV, the current across the pore is then expected to be 8.4 pA. This is about three times larger than the current measured experimentally in gramicidin A (Andersen, personal communication). This example illustrates that ion permeation across channels is not just a passive process as envisioned in Ohm's law—ions moving from one side of the membrane to the other under a uniform driving field, confined by the channel walls but not interacting with them. In fact, ions do interact with the fixed and induced surface charges on the channel walls that creates energy wells and barriers along the permeation path, the net effect of which is to attenuate the current from that of a purely passive pore. Thus, a correct calculation of the ion-channel interactions is of utmost importance in order to obtain reliable results from a permeation model.

Fick's law provides a similar relationship between the flux of ions and the concentration gradient across a channel

$$\mathbf{J}_n = -D\nabla n, \tag{4}$$

where D is the diffusion coefficient of ions. Here the subscript n denotes number flux which is related to the current density by $\mathbf{J}=e\mathbf{J}_n$. As shown by Einstein in 1905, the underlying physics is the same as in Ohm's law, namely, the Brownian motion of ions. In equilibrium conditions, the average positions of ions do not change but their root mean square distance from the initial positions grow with time as $\langle\mathbf{r}^2\rangle=6Dt$ due to the fluctuations. In the case of ion channels, when one side of the membrane has a higher concentration than the other ($n_1>n_2$), ions will flow to the other side with a flux, $\mathbf{J}_n=D(n_1-n_2)/L$, where L is the channel length. The above remarks about the channel not being a passive conduit for ions equally apply to such

simple applications of Fick's law, that is, ion-channel interactions will lead to a reduction in the flux obtained by assuming a passive pore.

In general, there could be both a potential and a concentration gradient driving the ions across an ion channel. This situation is described by the Nernst–Planck equation that combines Ohm's and Fick's laws

$$\mathbf{J}_n = -D\nabla n - \frac{g}{e}\ \nabla\varphi = -D\left(\nabla n + \frac{ne}{kT}\ \nabla\varphi\right). \tag{5}$$

In writing this expression, we have made use of the Einstein relation, $g = ne^2D/kT$, which relates the conductivity to the diffusion coefficient. Because the potential in an ion channel depends on the ion concentrations there, use of the Nernst–Planck equation with a predetermined or assumed potential is problematic. To avoid the question of self-consistency, one has to include contribution of the ions to the potential, which we discuss below. While the Nernst–Planck equation is primarily used to describe current flow, in the special case of a vanishing current, it makes an important statement about the electrochemical equilibrium in cells. Using $\mathbf{J}_n = 0$ in Eq. (5) and integrating once, we obtain the celebrated Nernst equation

$$\varphi_1 - \varphi_2 = -\frac{kT}{e}\ \ln(n_1 - n_2) = -59\ \log\frac{c_1}{c_2}\ (mV), \tag{6}$$

that gives the potential difference required to maintain the equilibrium when the concentrations are different on the two faces of the membrane. The numerical factor in Eq. (6) is obtained using $T = 298$ K. In practice, the Nernst equation is often used to estimate the membrane potential generated by asymmetric solutions in cells.

2.1.2. PNP equations

When ions move across narrow channels, they interact with the charge groups on the protein walls, and the electric potential at any given position changes due to their motion. To account for these effects, the potential on the right-hand side of Eq. (5) has to be calculated from Poisson's equation

$$\varepsilon_0\nabla\cdot(\varepsilon\nabla\varphi) = -(\rho_{\mathrm{el}} + \rho_{\mathrm{ex}}), \tag{7}$$

using the charge density due to both the mobile ions in the electrolyte, ρ_{el}, and other external sources such as fixed charges in the protein, ρ_{ex}. Here ε is the dielectric constant that has different values in water and protein. Once the appropriate boundary conditions are imposed at the water–protein interface, solution of Eq. (7) automatically takes into account the effects of "induced surface charges" (discussed in the following section). In the PNP theory, as the name implies, Poisson's equation is coupled to the Nernst–Planck equation, and the two equations are solved simultaneously, yielding the potential, concentration and flux of ions in the system. The two coupled equations are notoriously difficult to solve analytically, except for a few special cases (see Refs. [20,21] for a discussion of the analytical treatment of the PNP equations). With the advent of high-speed computers, the PNP equations can be readily solved numerically, enabling us to compute the current across ion channels. PNP is perhaps the simplest form of a nonequilibrium theory that takes into account the shape of the channel, the magnitude and location of charge residues in the channel protein, applied electric field and asymmetrical ionic concentrations in the two sides of the channel.

To calculate the current across a channel, it is placed in a simulation system, and a reservoir with a fixed number of ions is attached at each end of the channel. The simulation system is then divided into small rectangular grids, and the PNP equations are solved at grid points using a finite difference algorithm [22,23]. The grid size has to be optimized for an efficient running of the PNP program. A smaller grid size improves accuracy of the results but also takes a much longer computational time. The required inputs for the algorithm are: (i) the channel shape, (ii) the dimensions of the reservoirs and ionic concentrations in each reservoir, (iii) the dielectric constant of the protein and the solution, (iv) the locations and strengths of charges on the channel wall, (v) the membrane potential, and (vi) the diffusion coefficients of cations and anions. Once these parameters are specified, the solutions of the PNP equations give the concentration and potential throughout the system as well as the ionic currents through the channel.

2.1.3. Debye screening

To understand the range of validity of the PNP theory, and where and how it fails, we investigate the behavior of the two coupled equations more closely. Consider the potential at some point in a 1:1 electrolyte solution. The number densities of the positive and negative ions n_+ and n_- at that point are given by the Boltzmann distribution:

$$n_+ = n_0\exp[-e\varphi/kT], \quad n_- = n_0\exp[e\varphi/kT], \tag{8}$$

where n_0 is the average number density of ions in the solution. If φ is positive, there will be more anions, whereas if φ is negative, there will be more cations. The charge density in the electrolyte is the amount of excess positive or negative ions multiplied by charge per ion:

$$\rho_{\mathrm{el}} = e(n_+ - n_-) = -2n_0e\sinh(e\varphi/kT). \tag{9}$$

Expanding the sinh term in Eq. (9) and substituting only the leading term in φ in Poisson's Eq. (7), we obtain

$$\nabla^2\varphi = \kappa^2\varphi, \tag{10}$$

where κ^{-1} is the Debye screening length given by

$$\kappa^{-1} = \sqrt{\frac{\varepsilon_0\varepsilon kT}{2e^2n_0}}. \tag{11}$$

At room temperature ($T = 298$ K) and in water ($\varepsilon = 80$), the Debye length is related to the concentration as $\kappa^{-1} = 3.07/$

$\sqrt{c_0}$ Å, where c_0 is in M. Thus, for $c_0 = 0.15$, 0.5 and 1 M, the Debye lengths are, respectively, 7.9, 4.3 and 3.1 Å. The solution of Eq. (10) for a central test ion, also known as the Debye–Hückel theory [24], gives a clear physical picture of the behavior of ions in electrolyte solutions. When a cation is located at a fixed point, the density of anions around it increases, peaking at 1 Debye length or $r = \kappa^{-1}$, and then decays exponentially to the background number density. The Coulomb potential due to this test ion is shielded or screened by the excess of anions in the vicinity. The amount of screening of this potential rises monotonically, reaching 25% at 1 Debye length and 80% at 3 Debye lengths. Thus, for $c_0 = 150$ mM, length scales of about 30 Å are required for nearly complete screening of the Coulomb potential (or charge) of an ion.

2.1.4. Induced surface charges

The relevance of the Debye shielding arises from the fact that an ion near the protein induces surfaces charges of the same polarity on the protein–water interface. When a cation in an electrolyte solution is placed near a slab of protein, water molecules near the ion align themselves such that the oxygen atoms, with their partial negative charges, are positioned nearest to the ion. Because polar or carbonyl groups on the protein wall cannot rotate as freely as water molecules, there will be excesses of hydrogen atoms at the water–protein interface. Viewed from the ion, these excess hydrogen atoms at the boundary appear as surface charges, exerting a repulsive force on it. Macroscopically, we say that a charge q located at a distance d from a slab of protein surface induces surface charges on the dielectric boundary. For an idealized infinite plane, the magnitude of the repulsive force this ion experiences is the same as when we place another charge q', at the other side, at a distance d from the surface, and remove the boundary. The magnitude of this image charge q' is related to the relative permittivities of the protein ($\varepsilon_p = 2$) and water ($\varepsilon_w = 80$), given by

$$q' = \frac{\varepsilon_w - \varepsilon_p}{\varepsilon_w + \varepsilon_p} q. \tag{12}$$

As the ion comes nearer to the boundary, the repulsive image force it experiences grows as d^2. A similar repulsive force acts on an ion that is about to enter an ion channel. Only, the force is more than an order of magnitude larger in this case because the dielectric boundary is now wrapped around the ion, enhancing the effect. Thus, an ion entering a pore formed by membrane proteins encounters an energy barrier due to the induced surface charges, the height of which increases rapidly with decreasing radius of the pore. This energy barrier, sometimes called self-energy or reaction field, plays an important role in determining permeation properties of ions across a narrow pore. For example, saturation of conductance cannot be explained if one ignores the self-energy barrier of ions. One shortcoming of the PNP theory is in its failure to correctly calculate the magnitude of the induced surface charges and the resulting self-energy barriers.

2.1.5. Validity of the PNP theory

If the dimensions of the system one is dealing with is much larger than the Debye length, the PNP will give accurate results. As an example, consider ion diffusion across a cylindrical channel whose radius is 30 Å. The charge of an ion near the central axis of the pore will be completely screened by the counterions, so that there will be no induced surface charges on the water–protein boundary due to this ion. Thus, no self-energy barriers will be encountered by the permeating ions. In this situation, the PNP theory will correctly predict the current across the pore under various driving forces. Now, let us consider a similar cylindrical channel with a radius of 3 Å, spanning a 30-Å-thick membrane, whose volume is $\sim 10^3$ Å^3. At physiological concentrations, an anion or a cation is expected to be in this pore only 10% of the time on average. As an ion enters the pore, it induces surface charges of the same polarity, which exert a repulsive force on it, pushing it out. Normally, there are no counterions in the pore to screen its charge and hence cancel the repulsive force. In the PNP theory, the simulation system is divided into small cubic cells with a volume, say, 1 Å^3, each of which contains 10^{-4} of a cation and an equal fraction of an anion. The effect of the fractional charge in each grid on the protein wall is completely screened by the equal and opposite fractional charge present in it. These fractional charges diffuse across the pore, one cubic grid to the other, under the influence of the membrane potential, unencumbered by any induced surface charges on the protein boundary. In short, the ion–protein interaction, which is the dominant force in the process of ion permeation across a narrow pore, is completely ignored in the PNP theory.

Detailed studies comparing PNP with Brownian dynamics [23] and lattice Monte Carlo simulations [25] have revealed that the PNP theory can be reliably applied to study the permeation process across pores whose radius is about 2 Debye lengths (or 16 Å for a 150 mM solution). The magnitude of errors increases rapidly as the radius of the pore becomes smaller. Thus, application of PNP to biological ion channels, which have radii much smaller than 2 Debye lengths, is not justified. A second problem in this respect is how to treat the ion–ion interactions in PNP, which are known to play an important role in multi-ion channels such as potassium and calcium. These problems need to be resolved satisfactorily before PNP can be used to study the structure–function relations in ion channels.

2.2. Stochastic dynamics

2.2.1. Langevin equation

There are several tools in statistical mechanics that treat the dynamics of nonequilibrium systems, the most widely known is perhaps the theory of Brownian motion. The

behavior of an ion in an electrolyte solution undergoing a random type of motion can be described by the dynamical equation of motion in classical mechanics, known as the Langevin equation. The simplest form of stochastic dynamics, which deals with many-particle systems such as liquids and solutions, is Brownian dynamics. Brownian motion is triggered by the presence of a background noise or fluctuations and the energy gained by a Brownian particle is dissipated in the medium.

When an impulsive force is imparted on a macroscopic particle with mass m in a fluid medium, its subsequent motion is given by Newton's equation of motion

$$m\frac{\mathrm{d}\mathbf{v}}{\mathrm{d}t} = -m\gamma\mathbf{v}, \tag{13}$$

where γ is the friction coefficient, which is roughly proportional to the viscosity of the medium and the radius of the particle. The integral of Eq. (13) is simply given by $\mathbf{v}=\mathbf{v}_0 \exp(-\gamma t)$. Thus, the velocity of the particle exponentially decays to zero due to the frictional force. In other words, the energy of the particle is dissipated to the surrounding molecules in the fluid. For an ion in water, however, the situation is different because it has a similar mass as water molecules. The mean squared velocity of the ion in thermal equilibrium does not decay but remains at 3 kT/m (where k and T are the Boltzmann constant and temperature in Kelvin). This background motion of the ion is brought about by random forces, caused by incessant collisions with the surrounding molecules. Thus, a random or fluctuation force $\mathbf{F}_\mathrm{R}$ needs to be added to the right-hand side of Eq. (13) to account for the motion of an ion performing Brownian motion

$$m\frac{\mathrm{d}\mathbf{v}}{\mathrm{d}t} = -m\gamma\mathbf{v} + \mathbf{F}_\mathrm{R}. \tag{14}$$

Eq. (14), known as the Langevin equation, is the fundamental equation that describes the random motion of ions in an electrolyte solution. Both the dissipative and fluctuating forces stem from the same underlying mechanisms, namely, the random bombardment of ions by water molecules in thermal motion, and their interrelationship is described by the fluctuation–dissipation theorem of statistical mechanics [26].

The above description of the Langevin equation applies to ions freely diffusing in water. For ions in the vicinity of a channel, there is an additional, systematic force that influences their motion, namely, the electric force. It originates from four different sources. First, there is the electric field resulting from the membrane potential. Secondly, there are fixed charges in the channel protein and the electric field emanating from them will add to the field generated by the membrane potential. Thirdly, charges carried by all the ions in electrolyte solution contribute to the total electric field. Finally, whenever any of these ions comes near the protein wall, it induces surface charges of the same polarity at the water–protein interface. This last component of the force exerted on an ion plays a crucial role in influencing the motion of an ion attempting to traverse across a narrow pore formed by the protein wall. Each of these four components of the electric force acting on an ion needs to be computed, summed and added as a third term to the right-hand side of Eq. (14).

2.2.2. BD simulations in ion channels

To carry out Brownian dynamics simulations of ion channels, one needs to specify the boundaries of the system. This is a relatively simple problem for one-dimensional BD simulations [13,27,28], but requires addition of reservoirs to the channel system in the more realistic case of three-dimensional BD simulations. Here we describe a simple stochastic boundary that has been used successfully in applications of BD to a number of ion channels [29–33]. Large reservoirs with a fixed number of K^+ (or Na^+) and Cl^- ions are attached at each end of the channel. The membrane potential is imposed by applying a uniform electric field across the channel. This is equivalent to placing a pair of plates far away from the channel and applying a potential difference between the two plates. Assuming that the space between the electrodes are filled with electrolyte solutions, the potential drop occurs mainly across the channel. When an ion strikes the reservoir boundary during simulations, it is elastically scattered back into the reservoir. This operation is equivalent to letting an ion enter the reservoir whenever one leaves the simulation system. Thus, the concentrations of ions in the reservoirs are maintained at the desired values at all times. During simulations of current measurements, the chosen concentration values in the reservoirs are maintained by recycling ions from one side to the other whenever there is an imbalance due to a conduction event. This process mimics the current flow through a closed circuit.

The number of ions that must be placed in each reservoir for a chosen concentration depends on the size of the reservoir. Because the computational cost is directly proportional to the number of ions in the simulation system, it is desirable to have a small reservoir. At the same time, it must be large enough such that the ions in the system are in conditions similar to those in bulk electrolyte solutions. For example, the number of ions near the entrance of the pore should fluctuate according to the binomial distribution. To meet these requirements, an elaborate treatment of boundaries using a grand canonical Monte Carlo method was proposed [35]. Elsewhere it was shown that [36], provided the dimensions of the reservoirs are about 3–4 Debye lengths, the simple stochastic boundary as described above gives the same results as the more sophisticated method proposed in Ref. [35].

In BD simulations, the Langevin equation is solved repeatedly to trace the trajectory of every ion in the assembly. Snapshots of the simulation system are taken at short time intervals for millions of time steps. At each time

step, the Langevin equation is integrated to obtain the velocity of each ion to determine to which position the ion will move in the next time step. The new coordinates of all ions in the assembly are deduced, and the calculation is repeated. By repeating this process for a sufficiently long period of time, usually many microseconds, one can deduce how many ions move across the channel in a fixed period of simulation time. Because of the random and frictional forces, the methods for integrating Eq. (14) is complicated, and the reader is referred to Ref. [18] for details.

The choice of the time step is very important for the reliability of BD simulations. If the time step is chosen too short, the number of times the Langevin equation needs to be solved for a given simulation time increases. On the other hand, the accuracy is compromised if the time step is too long, although the computational cost is reduced. To understand how a particle undergoing Brownian motion behaves, we integrate Eq. (14) twice to obtain the expression for the mean square displacement [18]

$$\langle x^2 \rangle = \frac{2kT}{m\gamma} [t - \gamma^{-1}(1 - \exp(-\gamma t)]. \quad (15)$$

Here γ^{-1} is the relaxation time constant, which corresponds to the time required for a particle that is suddenly displaced to relax back to the original equilibrium position. For K^+ and Cl^-, γ^{-1} is about 30 fs. If we look at a potassium ion once every hundred of fs, (t is much larger than γ^{-1}), its mean square displacement becomes proportional to t

$$\langle x^2 \rangle = \frac{2kT}{m\gamma}\ t. \quad (16)$$

In other words, the ion behaves like a diffusing particle executing a random walk. In contrast, if we examine the same ion at short time intervals, say a few fs (t is much smaller than γ^{-1}), the mean-square displacement is

$$\langle x^2 \rangle = \frac{kT}{m}\ t^2. \quad (17)$$

That is, the ion in a short initial time interval behaves like a free particle moving with the constant thermal velocity of $(kT/m)^{1/2}$.

In implementing the BD algorithm for ion channels, we need to consider the behavior of ions in these short and long time intervals. When the force experienced by an ion is changing rapidly, as it is when the channel geometry undergoes sudden changes, it is desirable to use a short time step of 1–2 fs. On the other hand, a long time up to 100 fs can be used in the reservoirs with no loss of accuracy. In the algorithm of Chung et al. [31], a short time step of 2 fs is used when an ion is in the channel region where the force is expected to change rapidly, and a long time step of 100 fs is used when an ion is elsewhere. If an ion is in the channel at the beginning of a 100-fs period, it is simulated by 50 short time steps instead of one long time step; so synchronization among the ions is maintained. One can simplify the algorithm by omitting the inertial term $m[d\mathbf{v}/dt]$ from Eq. (14), and take time steps larger than the relaxation time constant. Because of its simplicity, this form is sometimes used in the literature [35]. Its applicability to ion channels, however, is limited because the rapidly changing forces inside a channel demand use of short time steps.

2.2.3. Validation of the BD algorithm

The behavior of the interacting ions deduced from the BD simulations accords with the physical reality. Fig. 1 shows the mean square displacement $\langle x^2 \rangle$, the velocity distribution, and the velocity autocorrelation function $\langle v(0)\, v(s) \rangle$ obtained from one simulation lasting 500,000 time steps. Theoretically, $\langle x^2 \rangle$ should be a linear function of time as given in Eq. (16). The measured slopes for Na^+ and Cl^- shown in Fig. 1A (solid lines) are about 7% lower than the predicted values for a bulk solution, which is due to ions scattering back from the boundary, retarding their free diffusion. The velocity distributions of Na^+ and Cl^- in the system are shown in Fig. 1B. From the equipartition theorem, these distributions should be Maxwellian. The measured distributions (circles) match closely those computed from the theoretical distribution (solid lines). Theoretically, the velocity autocorrelation function should be of the form:

$$\langle v(0)v(s) \rangle = \frac{kT}{m}\ \exp(-\gamma\, |\, s\, |\,). \quad (18)$$

Thus, regardless of the initial velocity, the successive velocities will be correlated over a time interval on the order of γ^{-1}, the relaxation time constant of the ion. The measured functions (circles) shown in Fig. 1C decay exponentially, as predicted from Eq. (18) (solid lines). Thus, we conclude that BD simulations can faithfully characterize the motion of ions in a solution confined to a small reservoir.

2.2.4. Uses of BD in ion channels

The ability to compute current flow across ion channels confers a distinct advantage to BD simulations compared to other simulation techniques. Thus, two obvious applications of BD in ion channels are the calculation of the current–voltage and conductance–concentration curves, which can be directly compared to the physiological measurements to assess the reliability and predictive power of the method. By simulating mixture of ions, one can also study selectivity ratios of ions. Since ions with the same valence are treated on an equal footing in BD, this can be used in a straightforward manner only in studies of valence selectivity. For monovalent ions, one has to supplement the potential profiles of ions with free-energy differences obtained from MD simulations.

In addition to simple counting of ions crossing the channel, one can carry out a trajectory analysis of ions in the system to determine their average concentrations. This is useful in finding the binding sites and the average number of

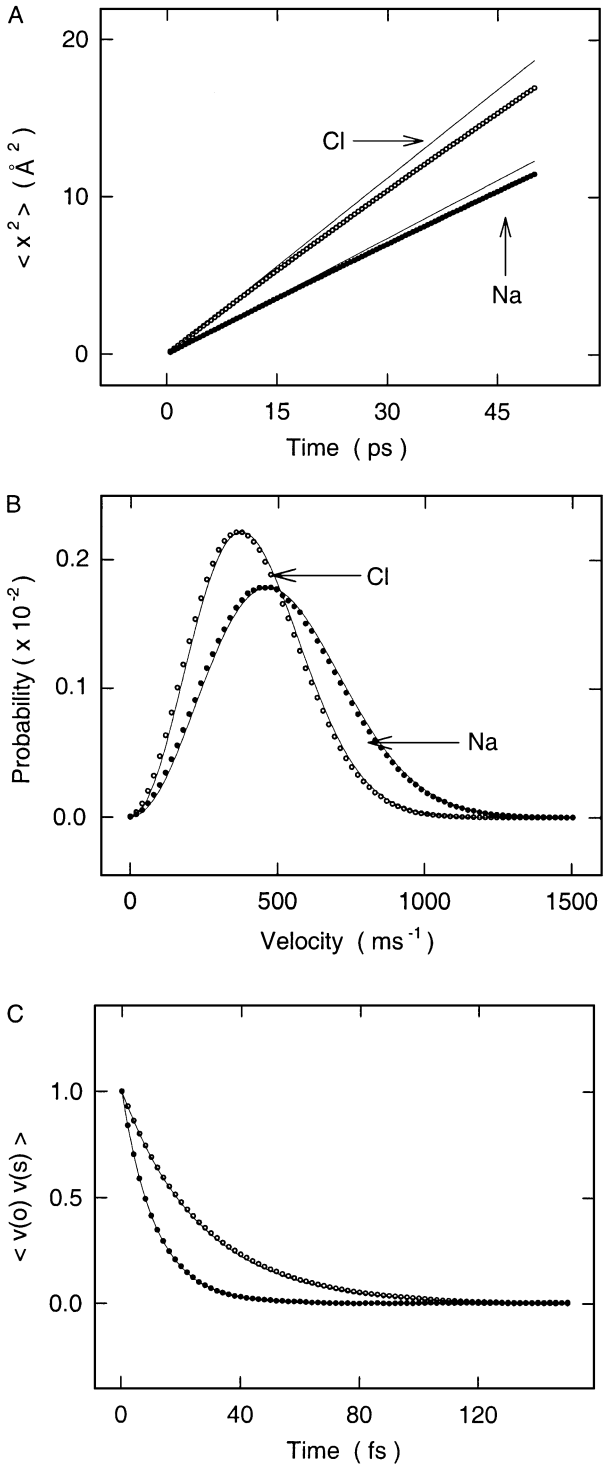

Fig. 1. Validation of the BD algorithm. Results of the BD simulations are indicated by ○ for chloride ions and ● for sodium ions. (A) Comparison of the mean-square displacements of ions with the diffusion formula, $\langle x^2 \rangle = 2Dt$ (solid line). (B) Comparison of the velocity distributions of ions with the Maxwellian distribution (solid line). (C) Comparison of velocity autocorrelation functions of ions with Eq. (18).

ions in the channel, both of which are experimentally observable quantities. Blocking of channels by larger molecules or divalent ions can be studied in a similar manner in BD. A prime example is the mole fraction effect, where increasing concentration of one type of ions leads to a reduction in the conductance of another. More refined analysis of BD trajectories can reveal the important transitions that take place during conduction events. This would be very important in interpreting the BD simulation results in terms of the rate theories. Alternatively, one can animate the trajectories of ions obtained from the BD simulations and directly watch the permeation of ions in real space time. This aspect of BD simulations will be discussed in the applications section below in more detail.

2.2.5. Limitations of BD

Ultimately, BD is a phenomenological theory with a number of assumptions and parameters that must be validated or derived from a more fundamental theory, such as MD. Treatment of water in a narrow pore as continuum is presumably the most drastic simplifying assumption of the BD method. The two basic parameters in BD simulations, namely, the dielectric constant of channel water and the diffusion coefficient of ions will certainly differ from their bulk values because of this confinement. Perhaps a more crucial issue is whether such a continuum approximation can be justified or not. MD studies of water confined in narrow pores have shown that the boundary imposes an order on the water molecules reducing their polarizability significantly [37–40]. On the basis of such studies, it has been argued that one should use very low values of ε for channel waters. However, such deductions for pure water are not quite relevant for ions because, from an ion's point of view, the role of the dielectric constant is simply to reduce its field by $1/\varepsilon$. So in choosing an effective ε value for channel waters, one has to address whether and by how much does the screening of an ion's field is reduced in a channel compared to the bulk environment. Dielectric screening is described by the first hydration shell in the Born model, which gives a successful account of the solvation energies of ions. Recent MD free energy calculations of solvation energies and solvent charge distribution around an ion have provided further microscopic support for the primacy of the first hydration shell [16]. Because the electric field of an ion in its first hydration shell is much stronger compared to any other source, one expects it to dominate the solvation dynamics regardless of whether the ion is in bulk or in a channel environment. Thus, as long as the first hydration shell of ions remains intact in a channel, use of continuum electrostatics with an ε closer to the bulk value may be justified. This criterion is generally satisfied in biological ion channels, including the narrow selectivity filter regions where protein atoms substitute for water completing the solvation shell. A rigorous justification of these ideas and extraction of effective ε values from MD simulations remain as future problems.

Another limitation of BD is the treatment of the water–protein interface as a rigid boundary. Proteins forming channels are certainly not static, but whether their motion

or flexibility plays an important role in ion permeation is not known. Since large conformational changes of proteins is a much slower process than ion permeation, such motions are not likely to be relevant. Local motions such as flipping of a side-chain are much faster and may play a role in ion permeation. This problem needs to be explored both experimentally and from MD simulations. If found to be important, such motions of the protein need to be incorporated in BD modeling of ion channels.

Finally, as pointed out above, size-dependent selectivity among ions with the same valence cannot be understood within the BD framework, and one has to appeal to MD simulations for that purpose.

2.3. Molecular dynamics

Use of MD in modeling of biomolecular systems has been growing continuously since the early eighties. Despite the complexity of performing MD simulations, availability of several user-friendly packages such as AMBER [41], CHARMM [42] and GROMOS [43] have made the MD method accessible to any researcher with a modest workstation. The increasing applications of MD in biology have raised the hopes that one can eventually study the biological processes at a microscopic level and relate the function of a protein complex to its underlying molecular structure. The resulting proliferation has also its downside as there are many difficult issues involved in ensuring the reality of results of an MD simulation [44]. Applications of MD to ion channels provide a case in point as will be discussed at some length below.

2.3.1. General formalism

In MD simulations, one follows the trajectories of N particles interacting via a many-body potential $U(\mathbf{r}_1, \mathbf{r}_2, \ldots, \mathbf{r}_N)$ using Newton's equation of motion:

$$m_i \frac{\mathrm{d}^2\mathbf{r}_i}{\mathrm{d}t^2} = \mathbf{F}_i, \tag{19}$$

where m_i and $\mathbf{r}_i$ denote the mass and position of the ith particle, and the force on it is given by the gradient of the potential U. Because all the atoms in the system (including water molecules) are represented explicitly in MD, there are no frictional or random forces to deal with as in BD. This makes the integration of Eq. (19) rather trivial. Given the positions and velocities of the particles at time t, at a later time $t+\Delta t$ they are updated to

$$\mathbf{r}_i(t+\Delta t) = \mathbf{r}_i(t) + \mathbf{v}_i(t)\Delta t + \frac{\mathbf{F}_i(t)}{2m_i}\Delta t^2,$$

$$\mathbf{v}_i(t+\Delta t) = \mathbf{v}_i(t) + \frac{\mathbf{F}_i(t)}{m_i}\Delta t. \tag{20}$$

In most MD programs, alternative forms of solutions are employed for convenience. For example, in the popular Verlet algorithm, the velocity term is eliminated from Eq. (20) by adding $\mathbf{r}_i(t-\Delta t)$ to $\mathbf{r}_i\,(t+\Delta t)$, which yields

$$\mathbf{r}_i(t+\Delta t) = 2\mathbf{r}_i(t) - \mathbf{r}_i(t-\Delta t) + \frac{\mathbf{F}_i(t)}{m_i}\Delta t^2. \tag{21}$$

Another widely used form is the leap-frog algorithm, where velocities are calculated at half intervals

$$\mathbf{r}_i(t+\Delta t) = \mathbf{r}_i(t) + \mathbf{v}_i(t+\Delta t/2)\Delta t,$$

$$\mathbf{v}_i(t+\Delta t/2) = \mathbf{v}_i(t-\Delta t/2) + \frac{\mathbf{F}_i(t)}{m_i}\Delta t. \tag{22}$$

The two forms are, in fact, equivalent as can be verified by substituting velocity in position in Eq. (22), and eliminating $\mathbf{v}_i\,(t-\Delta t/2)$ using the corresponding expression for $\mathbf{r}_i\,(t)$. At every time step, the potential function is recalculated using the new positions of the particles, and this process is iterated for a number steps until a statistically satisfactory data set is generated. The trajectory data thus generated are stored at certain intervals, which are analyzed later to determine the structural and dynamical properties of a system. Quantities such as free energy, mean-square displacement, radial distribution and other correlation functions are calculated from an ensemble average of several simulations.

The integration of the equation of motion is about the only simple aspect of MD compared to BD—everything else from the force fields and the boundary conditions employed to the analysis and interpretation of results are more involved. A major reason for this complexity is the long-range Coulomb interaction between the charged particles that normally comprises almost all the atoms in a biomolecular system. Here we briefly review those aspects of MD relevant to simulation of ion channels. For more details, the reader is referred to several textbooks on the subject [45–47].

2.3.2. Force fields

Since the force fields (or potential functions) are the crucial inputs in MD simulations, their correct choice is essential for a realistic simulation of a biomolecular system (see Ref. [48] for a recent review). If the atoms in a system could be represented as charged balls, they would simply interact via the Coulomb potential

$$U_{\mathrm{Coul}} = \frac{1}{4\pi\varepsilon_0}\,\frac{q_i q_j}{|\,\mathbf{r}_i - \mathbf{r}_j\,|}. \tag{23}$$

For two elementary charges, this potential energy amounts to $560/r$ kT when the distance r is taken in Å. In order to prevent atoms from overlapping, the Coulomb potential is usually supplemented with a hardwall potential. Unfortunately, the electrons around atoms are not inert but move

according to the quantum mechanical laws, which modify this simple classical picture in subtle ways. Incorporation of the effects of electrons in classical MD simulations has been an ongoing concern since the inception of the method in the 1960s. Electronic contributions to the intermolecular interaction can be divided into three groups: polarization, attractive dispersion (or van der Waals) and short-range repulsion.

The first term refers to the shift in the position of the electron cloud with respect to the nucleus when an atom is placed in an electric field. An exact description of polarization requires the solution of the Schrödinger equation for an atom in an electric field. Nevertheless, polarization can also be described using a simple classical picture where electrons move in a harmonic potential, provided the polarizability parameter α is taken from experiments. To leading order, an applied electric field $\mathbf{E}$ induces a dipole moment $\delta\boldsymbol{p}$ in an atom, given by

$$\delta\boldsymbol{p} = \alpha\boldsymbol{E}. \tag{24}$$

Higher order polarizabilities (e.g. quadrupole) are much smaller and usually neglected in simulation work. This induced dipole, in turn, creates an electric field of its own

$$\boldsymbol{E}_{\mathrm{pol}}(\boldsymbol{r}) = \frac{1}{4\pi\varepsilon_0}\,\frac{1}{r^5}\,[3(\delta\boldsymbol{p}\cdot\boldsymbol{r})\boldsymbol{r} - r^2\delta\boldsymbol{p}], \tag{25}$$

which further polarizes the surrounding atoms. Thus, polarization interaction is a many-body effect that needs to be taken into account self-consistently via iteration of the polarization and dipole field equations. Once a consistent set of induced dipole moments are determined for all the atoms in the system, the polarization contribution to the energy is given by

$$U_{\mathrm{pol}} = -\frac{1}{2}\sum_i \alpha_i \mathbf{E}_i\cdot\mathbf{E}_i^{(0)}, \tag{26}$$

where $\mathbf{E}_i$ denotes the total electric field at the site i and $\mathbf{E}_i^{(0)}$ is the field excluding the contributions of the induced dipoles, which correspond to the final and initial values of the field in the iteration process. Because this procedure is quite costly computationally, in most force field parametrizations, polarization effects are incorporated implicitly by invoking a mean field approximation. That is, an average induced dipole term is added on top of the monomer value so as to reproduce the bulk properties of a system. To give an example, the dipole moment of water is taken as ~ 2.3 D in popular water models such as SPC [49] and TIP3P [50], which is substantially larger than the experimental value of 1.85 D.

The second term, dispersion forces, arise from quantum fluctuations that leads to correlations between the electrons of two atoms. Virtual excitations of electrons in one atom generate a spontaneous dipole moment that polarizes the neighboring atoms yielding an induced dipole-induced dipole interaction. An approximate derivation due to London [51] gives for the dispersion potential between two like atoms

$$U_{\mathrm{disp}} = -\frac{3\hbar\omega_0\alpha^2}{4r^6}, \tag{27}$$

where r is the distance between the atoms and $\hbar\omega_0$ is an average electronic excitation energy. More accurate treatments that include the higher order induced multipole moments lead to a power series in $1/r^n$ with $n=6, 8, \ldots$ Unlike polarization, dispersion force is a purely quantum phenomenon with no classical analogue. For example, there are no polarization forces between neutral atoms but they are still attracted by the dispersion forces.

The last term has its origins in the Pauli exclusion principle that forbids two electrons occupying the same quantum state. When two atoms come into contact, the orbitals of electrons starts overlapping, which leads to a sharply rising repulsive potential. Since the tails of the electronic wave functions have an exponential radial dependence, a suitable form for this potential would be $A\exp(-r/a)$. However, the rational algebraic form A/r^{12} is often preferred in practical applications for computational convenience. In fact, combining the dispersion and repulsive potentials in a so-called Lennard–Jones (LJ) 12–6 interaction has become almost an industry standard in MD force fields

$$U_{\mathrm{LJ}} = 4\epsilon[(\sigma/r)^{12} - (\sigma/r)^6]. \tag{28}$$

Here ϵ is the depth of the potential at the minimum ($r_{\min}=2^{1/6}\sigma$), and σ is where the potential vanishes. This form reduces the number of free parameters by one and it appears to provide an adequate description of solutions. Compared to the Coulomb and polarization interactions, the LJ potential is weaker and has a much shorter range ($\epsilon \ll 1$ kT and σ is in the range of 2–4 Å for most atoms). The LJ potentials between different atoms are determined from those between the like atoms using simple combination rules such as taking the geometric mean of the parameters

$$\epsilon_{ij} = \sqrt{\epsilon_{ii}\epsilon_{jj}}, \quad \sigma_{ij} = \sqrt{\sigma_{ii}\sigma_{jj}}. \tag{29}$$

Alternatively, one can use the arithmetic mean of the LJ distance parameter σ, $\sigma_{ij}=(\sigma_{ii}+\sigma_{jj})/2$ while keeping the geometric mean for ϵ.

As stressed above, in most force fields the polarization interaction is neglected, and the parameters in the Coulomb (partial charges on atom centers) and the LJ interactions are determined from fits to the bulk properties (e.g., enthalpy of vaporization and density for water). We remark that the pair potentials determined in this way incorporate many other effects in their parametrizations, and therefore do not have much in common with the actual dimer interaction in vacuum. The justification for such a simplified phenomenological approach ultimately comes from its success in

reproducing experimental observations. In this regard, more fundamental approaches based on accurate many-body interactions have been much less successful [52].

The above description of forces applies to nonbonded interactions among water molecules and ions in an electrolyte solution. The atoms in proteins and lipids that form the rest of the system in ion channels are not free but bonded to their nearest neighbors by covalent interactions. Three types of bonding interactions are typically employed for this purpose: stretching of a bond length r between two atoms, bending of a bond angle θ formed by three atoms and torsion of a dihedral angle between the 123 and 234 planes of four atoms. The first two are represented by harmonic potentials

$$U_{\text{bond}} = \sum_{\text{bonds}} \frac{k_r}{2}(r_{ij} - r_{ij}^0)^2,$$
$$U_{\text{bend}} = \sum_{\text{angles}} \frac{k_\theta}{2}(\theta_{ijk} - \theta_{ijk}^0)^2, \quad (30)$$

where r_{ij}^0 and θ_{ijk}^0 are the equilibrium values for the bond lengths and angles, and k_r and k_θ are the corresponding force constants. The torsion potential is needed to describe the relative position of a third neighbor with respect to the plane defined by the first two, which cannot be achieved by the bending potentials alone. Because of the rotational symmetry, it has to be written in terms of periodic functions, a commonly used form being

$$U_{\text{torsion}} = \sum_{\text{dihedrals}} k_\phi(\cos(n\phi - \phi^0), \quad (31)$$

where k_ϕ is the force constant, ϕ^0 is the phase and n determines the periodicity of the potential.

The bonding interactions confer a certain degree of flexibility to the protein atoms forming an ion channel, which may change their configuration in response to a permeating ion. Unfortunately, with the currently available run times, this question is very difficult to address via direct MD simulations. Thus, it remains an open question whether protein flexibility plays an important role in ion permeation or correlations between the two are negligible.

2.3.3. Boundaries

A major problem in MD simulations is how to achieve a bulk-like environment when using a relatively small system, where surface effects invariably dominate. To give an example, for 1000 atoms in a box, about half of the atoms are in direct contact with the surfaces. This number drops to about a quarter for 10,000 atoms, which is still a significant percentage. Naturally, to avoid the surface effects, one needs to exclude more than one layer of atoms, which reduces the number of atoms in a bulk-like environment very rapidly in these systems. The traditional way to avoid the surface effects is to impose periodic boundary conditions. That is, the simulation system is replicated in all directions filling the whole space. Such a boundary condition is obviously desirable for crystals and seems to be a reasonable choice for solutions. For a grossly inhomogeneous system such as ion channels, periodicity introduces its own artifacts. These artifacts can be monitored by checking the dependence of results on the system size, though such precautions are rarely exercised in practice because of the time required. It is expected that the errors introduced by periodicity are much less severe than those that would result from the use of vacuum as a boundary. As a result, the periodic boundary conditions are adapted almost universally in current MD simulations of biomolecules as a lesser evil. A better justification for its use in simulations of ion channels is needed to substantiate accuracy of the current MD results.

The choice of periodic boundary conditions raises the question of how to handle the long-range Coulomb forces in the resulting infinite system. In earlier simulation work, cutoffs were often employed to truncate the Coulomb forces beyond a distance of ~ 10 Å. Lack of computer power was the main reason for using cutoffs, though reducing artifacts associated with periodicity was also cited as a justification. Increased computer power and development of fast algorithms that can evaluate the Coulomb interactions accurately have solved this problem in the last decade. Many comparisons carried out since then have shown the inadequacy of using cutoffs especially in systems containing charged particles [53]. The two main methods used for this purpose are Ewald summation and fast multipole method. In Ewald sum [54], the Coulomb interaction is split into a long and a short-range part using the identity involving the error function and its complement, $\text{erf}(\beta r) + \text{erfc}(\beta r) = 1$. Since $\text{erfc}(x)$ behaves like $\exp(-x^2)$ for large x, the short-range part (also called real-space or direct-space part) can be calculated accurately using a cutoff of ~ 10 Å. The long-range part is evaluated in the reciprocal space using Fourier transformation. Ewald sum reduces the computational cost from N^2 to $N^{3/2}$ for N charges, which is still considerable for large systems. The speed of the Ewald sum evaluations can be increased substantially by using particle-mesh based approaches that exploit the advantages of fast Fourier transform in calculating the long-range part [53]. These algorithms scale as $N\log N$ and have finally enabled accurate calculation of Coulomb forces in large systems. The fast multipole method is based on multipole expansion of the Coulomb potential in spherical coordinates. It is less efficient than the particle-mesh Ewald method and has not been widely adapted in MD packages.

2.3.4. Uses of MD in ion channels

Conductance is the primary observable in ion channels and one would like to be able to predict it within the MD framework. Unfortunately, this is not feasible with the current computer speeds. Because the rotational motion of water molecules is quite fast, one has to use a very small time step ($\Delta t \approx 1$ fs) in the numerical integration of Eq. (20) in order to maintain accuracy. Thus, an MD

simulation lasting a million time steps covers only 1 ns, which is too short to study conduction of ions in biological channels. A typical channel current of 5 pA corresponds to an average transit time of 32 ns for a single ion, and an MD simulation lasting ~ 1 μs is needed to obtain a sufficiently accurate conductance measurement. A few attempts have actually been made to compute the conductance of porin [55] and artificial channels [56] using relatively high applied potentials in the range of 0.5–2 V. However, because the $I–V$ curves are highly nonlinear, it is not clear how these results can be extrapolated to the physiological range of ~ 0.1 V.

In the absence of conductance, the quantity that provides the most useful information on permeation dynamics is the potential of mean force (PMF) of an ion calculated along the permeation path. Just like the potential energy profile of an ion in continuum electrostatics, PMF provides the work required to push the ion through the channel. Thus, the wells in a PMF point to the binding sites in a channel and barriers can be used in estimating its transit rate. The PMF can be calculated most simply from the definition of work as a line integral of force. The mean force on a test ion at a fixed position is determined from an ensemble average of several MD simulations. This process is repeated along the permeation path at small steps (~ 0.1 Å), and integration of the mean force along the path yields the PMF. For simple systems such as electrolyte solutions, this method is quite adequate and has been used to determine the PMF between ion pairs in an electrolyte solution [57,58]. Alternatively, one can use the definition of PMF in terms of the distribution function ρ, $W=-kT\ln\rho$. Obtaining an accurate sampling of the configuration space within a relatively short simulation period presents a problem for this method. This is circumvented by introducing a bias potential that enhances the sampling of the desired configuration, whose effects are removed later (umbrella sampling) [59]. The second method is more appropriate for complex systems containing proteins and lipids, and has been used in calculations of the PMF of ions in the gramicidin A channel [60].

The selectivity sequences among monovalent cations can be predicted in MD from the free-energy perturbation calculations. Because this quantity involves the energy difference for transformation of an ion of one type into another at the same location, inaccuracies in force fields are likely to cancel out, making such predictions more robust compared to the calculation of the free-energy profiles of an ion along the permeation path. Moreover, ions with the same valence cannot be distinguished in BD; hence, MD offers the only method for understanding their selectivity sequences. Diffusion coefficient of ions and dielectric constant of water in the channel are two other local properties that could be estimated from MD. These quantities are required as input parameters in BD simulations that would have to be determined from fits to experimental data otherwise. Thus, MD plays a complementary role to BD in many respects, reducing the arbitrariness in the choice of free parameters that so often plagues application of phenomenological models to realistic systems.

2.3.5. Limitations of MD

The currently available simulation times is presumably the greatest limitation of MD. While calculation of PMF provides useful information on ion permeation, it is not a substitute for a direct estimation of conductance from simulations. In the final analysis, the ultimate judge of the reality of a computer simulation is comparison with the experimental data. Without such comparisons, one has no way of knowing whether the results of an MD simulation reflects the reality or is an artifact of the method. With the doubling of computer speeds every 2 years, this time limitation will be eventually surmounted. In the meantime, the coarse-grained but much faster BD simulations need to be used to calculate the conductance of biological ion channels. An alternative approach may be provided by a combination of the BD and MD methods that will permit faster simulation of the atoms in regions of marginal interest without loss of accuracy for those in regions of focus. While this approach is very appealing, handling of the interface between the two regimes poses a problem that needs to be resolved before it can be applied to ion channels.

Considering the simplicity of the potential functions in current use, MD techniques have been remarkably successful in studies of lipid–protein systems. This suggests that the neglected terms in the potential—most notably induced polarization—are incorporated in the two-body terms such that their average effects are represented quite well. This average treatment of polarization appears to work well as long as one retains the bulk-like environment for the molecules in question [52,61]. In application of MD to ion channels, however, there is likely to be problems in this regard because ions move from bulk water into a narrow pore formed by protein molecules with very different polarization characteristics. Indeed, PMF calculations in the gramicidin A channel predict 20–30 kT barriers [15,62,63], which would make the channel impermeable to ions. Thus, the force fields currently employed in most MD programs appear not to be sufficiently accurate for the purpose of studying ion permeation in channels, and construction of new, polarizable force fields is desirable. A longer term goal is to use ab initio MD methods to derive the force field parameters directly from the electronic structure calculations rather than determining them empirically from fits to data [18]. There has been a great deal of progress in application of ab initio MD methods since the adaptation of the density functional theory [64] to calculate the potentials between atoms on the fly [65]. Initial applications of ab initio MD were in condensed matter physics, though in recent years, it has also been used in studies of water, electrolytes and biological molecules [18]. Modeling of ion channels is a natural step in this progression that presents a challenging problem for ab initio MD.

3. Computational studies on ion channels

All three permeation theories reviewed in the last section have been applied to ion channels. However, because of the shortcomings of the PNP approach outlined above, we consider only applications of the BD and MD methods in the following case studies. Of the channels with a known structure, KcsA potassium channel, is by far the most interesting case, and will be discussed in some detail. This is followed by gramicidin A because it has been the most studied channel model. Finally, we discuss the calcium channel as an example of how one may proceed in cases where there is limited structural information.

3.1. KcsA potassium channel

The unravelling of the crystal structure of the KcsA potassium channel by Doyle et al. [3] at 3.2 Å resolution is a landmark event that will have a lasting impact on ion channel studies. This is the first biological ion channel whose tertiary structure is elucidated. Therefore, it has prompted a flurry of theoretical investigations on the mechanisms underlying the permeation of ions across the channel, the basis of ion selectivity, and the conformational changes that occur in the KcsA protein when the channel opens. Very recently, MacKinnon et al. [66,67] succeeded in refining the crystal structure of KcsA to 2.0 Å, which allowed direct observation of the binding sites of K^+ ions in and near the selectivity filter, as well as the water molecules that are coordinated with these K^+ ions. These latest results could have ramifications in much wider fields as they turned the KcsA channel into a microscopic laboratory for studying the ion–water–protein interactions.

The KcsA structure determined from X-ray diffraction consists of 396 amino acid residues, or 3504 atoms excluding polar hydrogens [see Video Clip #1]. The channel is constructed by four subunits of a tetramer of peptide chains, each subunit consisting of an outer helix, inner helix, pore helix, and a TVGYG amino acid sequence that forms the selectivity filter. The protein atoms form a central pore between these subunits. An outline of this pore reveals that the channel is composed of three segments—a long intrapore region of length 20 Å lined with hydrophobic amino acids extending towards the intracellular space, a wide water-filled chamber of length 10 Å, and a narrow selectivity filter of length 12 Å extending towards the extracellular space (Fig. 2). The selectivity filter is the most important element in this structure as it can distinguish K^+ ions from those of Na^+ on the basis of their sizes (crystal radius of K^+ is 1.33 Å and that of Na^+ is 0.95 Å).

In the crystal structure, K^+ ions are observed to occupy four sites in the filter region with approximately equal probabilities [66]. These sites are in between the planes defined by the carbonyl and hydroxyl oxygens of the Y78, G77, V76 and T75 residues. Thus, a K^+ ion in one of these sites is solvated by eight oxygens from the neighboring

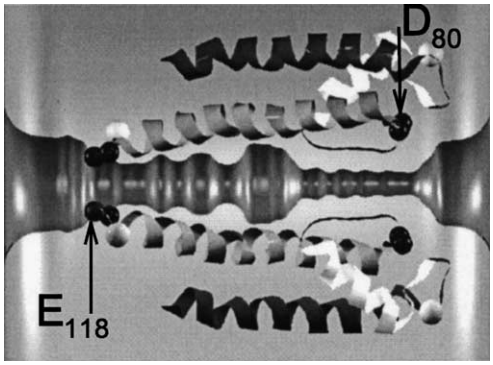

Fig. 2. Structure of the KcsA channel. The intracellular gate of the pore was widened using molecular dynamics simulations. Four glutamate residues (E_{118}) and four aspartate residues (D_{80}) are located near the intracellular and extracellular entrances of the pore, respectively.

residues. A similar eight-fold coordination of ions with water molecules is observed in the cavity and at the extracellular mouth of the channel [67]. These results are interpreted as two K^+ ions, with a water molecule between them, permanently occupying either the sites 1–3 or 2–4, and oscillating between these two configurations without any significant free energy barriers. Appearance of a third K^+ ion in the filter disrupts this equilibrium, starting a conduction event. The fact that K^+ ions are eight-fold coordinated with oxygen atoms at all sites from entry to exit makes the permeation process through the filter energetically very smooth, especially during the critical dehydration and rehydration steps.

The KcsA potassium channel is known to be activated at low intracellular pH [68,69] Paramagnetic spin resonance studies [70–72] have indicated that the KcsA crystal structure corresponds to a closed conduction state and the transmembrane helices forming the intracellular pore move away from the channel axis during gating. Also, in the crystal structure, the radius of the narrowest section of the pore on the intracellular side is 1.2 Å, smaller than the radius of the potassium ion (1.33 Å).

3.1.1. MD studies

Appearance of the KcsA structure has prompted many groups to investigate ion permeation in potassium channels using MD simulations. The main focus of these studies has been the selectivity filter and understanding the permeation properties of K^+ ions in the filter and cavity regions. Treatment of the membrane is a major problem in MD simulations of ion channels, and there has been a wide variation among various studies of the KcsA channel in this respect. In the most sophisticated ones [73,74], the KcsA protein is embedded in a DPPC bilayer and solvated with a 150 mM KCl solution. In a similar study [75], a POPC bilayer was employed with a varying number of K^+ ions. Because explicit simulation of lipid bilayers is computationally expensive, in most MD studies, they are represented with octanes [76,77] and nonpolar atoms [78–80], or more simply by harmonic constraints applied to the protein atoms

[81–84]. Simplified representations of bilayer enables longer simulations necessary for a detailed study of ion dynamics in the channel. Therefore, it would be worthwhile to find appropriate sets of constraints that can mimic the embedding of the KcsA protein in a lipid bilayer.

The MD simulations performed so far agree with the stable occupation of the channel with three K^+ ions, two in the filter and one in the cavity, as observed in experiments [3,66,67]. There is also some evidence that approaching of the K^+ ion in the cavity to the selectivity filter triggers a conduction event, and permeation across the filter occurs through the recycling of ions as $2K^+ \rightarrow 3K^+ \rightarrow 2K^+$ [73,74,78]. In particular, PMF calculations with multiple K^+ ions in the filter indicate that the free energy barriers between the binding sites remain around 3–4 kT, consistent with the estimates from experiments [74]. The question of selectivity against Na^+ ions has been addressed in several studies through free-energy perturbation calculations, where a K^+ ion in one of the binding sites is alchemically transformed into a Na^+ ion [see Video Clip #2]. The calculated free-energy barriers range from 11 kT [74] to 8 kT [82], and 5 kT [80], which are in rough agreement with the experimental value of $\sim$ 9 kT extracted from the K^+/Na^+ selectivity ratio of $\sim 10^4$. As stressed before, energy differences are less sensitive to inaccuracies arising from the use of nonpolarizable force fields, making these predictions more reliable.

Diffusion of ions and water in the KcsA channel have been studied by Allen et al. [81,82,85] and Biggin et al. [83]. The main finding from these studies is that the diffusion coefficient of K^+ ions is suppressed down to about 10% of the bulk value in the filter region but remains relatively high (>50% of the bulk value) in the rest of the channel. The hydrophobic residues lining the intrapore and cavity regions are responsible for the relatively high diffusion of ions in those segments. Despite the large suppression of the diffusion coefficient in the filter region, permeation through this segment turns out to be the fastest step in a full conduction cycle, thanks to the Coulomb repulsion. These results provide inputs for the BD simulations as discussed below.

Motions of individual ions in the channel have also been discussed in MD studies of KcsA. Most of these involve short time simulations of the concerted motions of the K^+–W–K^+ complex in the selectivity filter. In one MD study, a K^+ ion originally placed in the cavity was observed to exit to the intracellular space in 1 ns [75]. This appears to be a very fast event considering that the channel structure employed corresponded to a closed state and there was no applied potential. In any case, such single-event studies have little meaning statistically, and should not be used to draw conclusions about the permeation dynamics.

3.1.2. BD studies of ion permeation

Of the two common approaches used to model the potassium channels, MD simulations are incapable of simulating ion permeation for periods long enough to measure channel conductance. To determine currents flowing across the channel, Chung et al. [31,33,34] and others [86,87] have carried out BD simulations on the KcsA channel using the experimentally determined channel structure. In these simulations, water is treated implicitly as a continuum, and the protein atoms forming the channel are assumed to be rigid. With these simplifications, they were able to relate the channel function to its structure.

BD simulations show that [see Video Clip #3] there are three regions in the selectivity filter and cavity where K^+ ions dwell preferentially, as illustrated in the histogram in

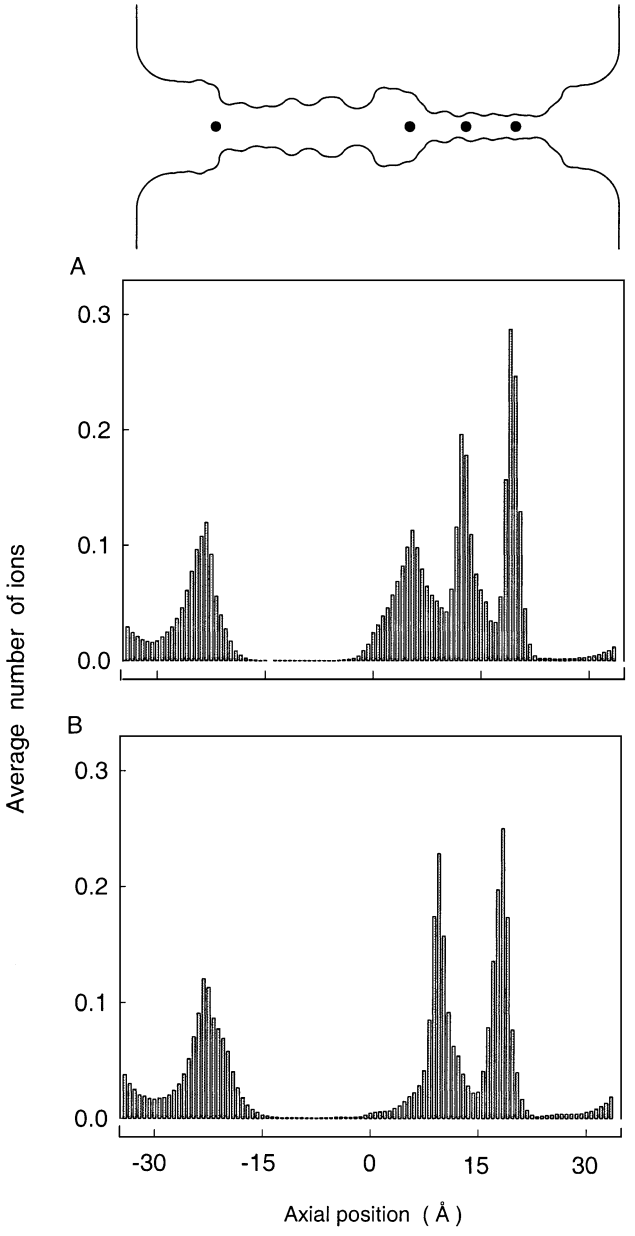

Fig. 3. Average number of ions in the channel with no applied field (A) and with an applied field of 10^7 V/m (B). The channel is divided into 100 sections, and the average number of ions in each section is calculated over a simulation period (0.1 μs). The outline of the channel and the approximate locations of ions in the absence of an applied field are shown in the inset.

Fig. 3A. The locations of their maxima are indicated schematically in the inset. There is also another prominent peak in the histogram, centered near the intracellular entrance of the channel. The average number of ions is 2.9 in the selectivity filter and the cavity, and 0.9 near the intercellular entrance. The preferred positions where ions dwell preferentially are in close agreement with the positions observed in Rb^+ X-ray diffraction maps [3]. When a potential difference is applied such that ions move steadily across the channel, the peak positions in the histogram shifts, as illustrated in Fig. 3B. There are now two prominent peaks in the selectivity filter region and one peak, as before, in the intracellular entrance. The average number of ions in the selectivity filter and cavity is reduced to 2.2, whereas that near the intracellular entrance increases to 1.2.

To illustrate the permeation mechanism implied by the BD results, we divide the channel into two halves such that ions in the chamber and filter are consigned to the right side, an the rest to the left side. For example, the most common situation in the conducting state of the channel has one ion on the left half, and two ions in the right half, and we refer to this as the [1, 2] state. A typical conduction event consist of the following transitions: [1, 2] → [0, 3] → [0, 2] → [1, 2]. In other words, the ion waiting near the intracellular mouth overcomes a small energy barrier in the intracellular pore to enter the chamber region. Because this system is unstable in the presence of an applied potential, the right-most ion is ejected from the channel. Another ion enters the intracellular mouth, leaving the system in its original configuration. Naturally, conduction of ions depends on their concentration, applied potential and the ionization state of the charged residues at the channel entry, and many other states can be involved in the conduction process depending on the values of these variables. For example, at high concentrations and potentials, a likely event follows the transitions: [1, 2] → [0, 3] → [1, 3] → [1, 2]. A common feature of all these conduction events is that the presence of 3 K^+ ions on the right side of the channel triggers a conduction event. This prediction of the BD simulations on the mechanism of ion permeation across the filter region has been confirmed by the latest experiments on the KcsA channel [66].

In Fig. 4A,B, we display the current–voltage and current–concentration curves obtained from BD simulations [33]. The outward conductance at 140 mV is 35 pS, increasing to about 65 pS at 250 mV. The relationship is linear when the applied potential is in the physiological range ($V < 150$ mV) but deviates from Ohm's law at a higher applied potential. The current saturates with an increasing ionic concentration, as shown in Fig. 5B. This arises because ion permeation across the channel is governed by two independent processes: ions accessing of the channel entry depends inversely on the concentration while their transit across the channel is independent of the concentration. As an example, we give the average times it takes for an ion to move through the various sections of the channel with an applied potential

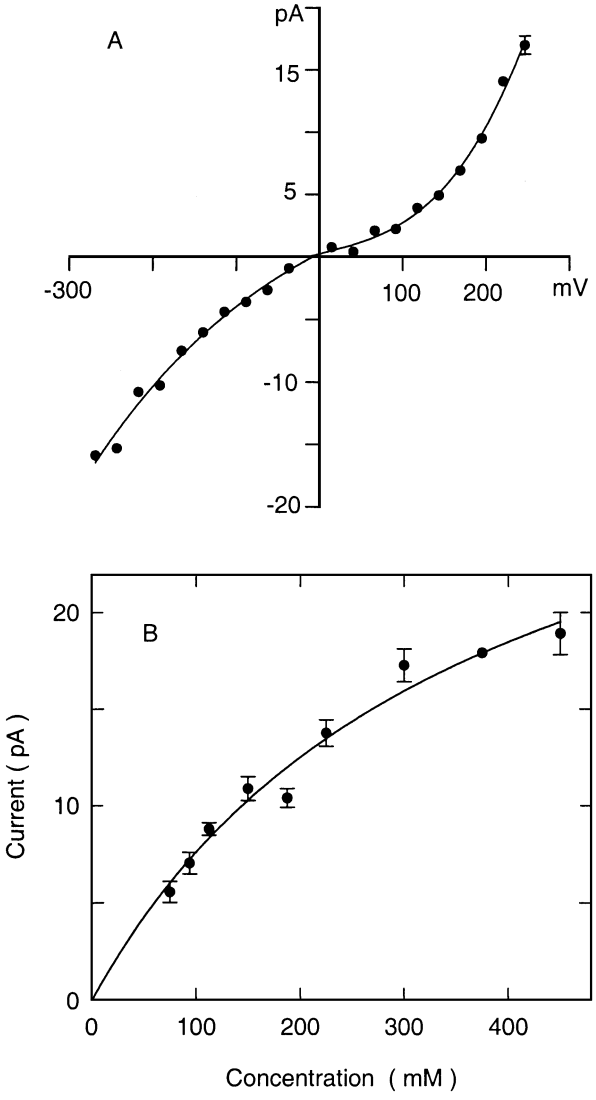

Fig. 4. The current–voltage (A) and current–concentration (B) curves obtained from BD simulations.

of 250 mV and concentration of 300 mM: the time it takes for an ion to enter the channel from the intracellular side is about 5 ns, the time for this ion to transit across the channel to reach the cavity is 6 ns, and finally, the time for the right-most ion to exit the filter is less than 1 ns. The last two processes, being independent of concentration, are the rate-limiting steps in conduction at high concentrations. It is worth emphasizing that permeation across the filter is much faster than in other parts of the channel. Thus, although the filter plays a crucial role in selecting the K^+ ions, its role in influencing their conductance properties is minimal. The conductance of the potassium channel and the shape of the conductance–concentration curve shown in Fig. 4 are in broad agreement with those determined experimentally [68,69,88–92].

The above result that shows the selectivity property is decoupled from the other physiological properties, offers a natural explanation for a well-known paradox in the potassium channel family, namely, despite the fact that the filter

sequence is conserved in all potassium channels [93–95], individually they exhibit very diverse conduction rates. This has important ramifications for modeling of other potassium channels because one can start from the KcsA structure as a template. A first step in this direction was taken by Chung et al. [34], who constructed a simplified model of KcsA that reproduced the calculated properties of the atomic-detail model, and studied how changes from this structure influenced its permeation properties. They found that changing the radius of the intrapore region from 2 to 5 increased the channel conductance by nearly two orders of magnitude, sufficient to explain the range observed in nature. This gives hope that individual potassium channels can be modeled using BD by taking into account available structural and physiological data. In this respect, homology and MD modeling of different potassium channels based on the KcsA structure could provide valuable clues [96,97]. Another important source of information is site directed mutagenesis, which can help to identify the charge residues that influence the permeation characteristics of a channel [98,99]. The recent modeling of calcium channels provides an apt illustration of this point that we discuss below.

3.2. Gramicidin A channel

In membranes, the dimer of the antibiotic peptide gramicidin A (GA) forms a cylindrical channel with length 25 Å and radius 2 Å, that selectively conducts monovalent cations. Its physiological properties are characterized by linear $I–V$ curves and relatively large half-saturation concentrations. These observations point to lack of substantial barriers within the channel. In addition, NMR studies indicate well established binding sites near the pore entrances. This wealth of functional data has been matched with an atomic resolution structure since 1971 [100]. For these reasons, the GA channel have played a prominent role in development of permeation models in ion channels. There is an extensive literature on modeling of the GA channel, which can be traced from several review articles [14,15,101,102]. Here we give a summary of the current situation with regard to applications of MD simulations to the GA channel, and comment on the relevance of such investigations on modeling of biological ion channels. Because inapplicability of continuum electrostatics to the GA channel was demonstrated in a recent work [103], such applications are not considered.

Free-energy profiles of ions calculated along the axis of the GA channel provide the most important information about permeation dynamics. To date, all such MD calculations have lead to central energy barriers that are too high to allow ion permeation through the GA channel at the observed rates. To give an example, the lowest translocation barrier calculated for Na^+ ions is about 20 kT [63], which would completely suppress flow of ions. Binding site locations at the channel entrance are generally reproduced by these profiles but again the absolute well depths do not appear to be consistent with the experiments. The selectivity sequences among monovalent cations, calculated from the free-energy differences, are in agreement with the experimental sequence $Cs^+>K^+>Na^+>Li^+$ [104,105]. That is, the larger ions with smaller hydration energies conduct better just as in bulk electrolytes. A common prediction of all MD simulations is that the backbone of the GA peptide exhibits some flexibility with the carbonyl oxygens swinging up to 10–20° [60,62] to provide adequate solvation for a nearby ion. Recent high-resolution NMR studies of cation transport in the GA channel [106,107] find that the GA peptide remains rather rigid upon cation binding and the ion is solvated by just two carbonyl oxygens and two water molecules. The loss in ion coordination number from 6 in bulk to 4 is significant because the missing solvation energy has to come from another source. One possible scenario is that the water molecules in the channel have, in fact, a more ordered structure than predicted by the current MD models of GA. Such an order could be induced by polarization interactions that would lower the energy of the ion-water column in the channel substantially.

Taken together, the above results point to potential problems with the force fields currently employed in the MD simulations. Thus, development of new force fields that take into account polarization effects should be a priority area in future studies. Unfortunately, with the appearance of the KcsA channel structure, GA has lost its once prominent status in the field. Nevertheless, because the GA channel has such a simple structure and is so rich in physiological data, it can still play an important role in the development of permeation models. After all, if a model works in the more complicated case of KcsA but fails in GA, it would lose much from its credibility.

3.3. L-type calcium channel

Calcium channels are as common as potassium channels and have many similar properties. They are extremely selective against Na^+ ions and exploit a multi-ion Coulomb repulsion mechanism to achieve a high throughput of Ca^{2+} ions [108]. The fact that Ca^{2+} and Na^+ ions have similar radii but different charges indicates that, unlike potassium channels, selectivity must be based on charge. Another difference of the selectivity property from the potassium channels is that it is contingent upon the presence of Ca^{2+} ions in the channel, and in their absence, Na^+ ions conduct at an even faster rate than Ca^{2+}. These observations suggest that one may be able to explain the selectivity of calcium channels within the BD framework without having to appeal to MD. Since the tertiary structure of the calcium channels are not known, this indeed appears to be the only way to study the structure–function relationships in this important class of channels. A first attempt to model the L-type calcium channel using BD was made by Corry et al. [32], who used the available information on its structure and conductance properties to construct a model channel con-

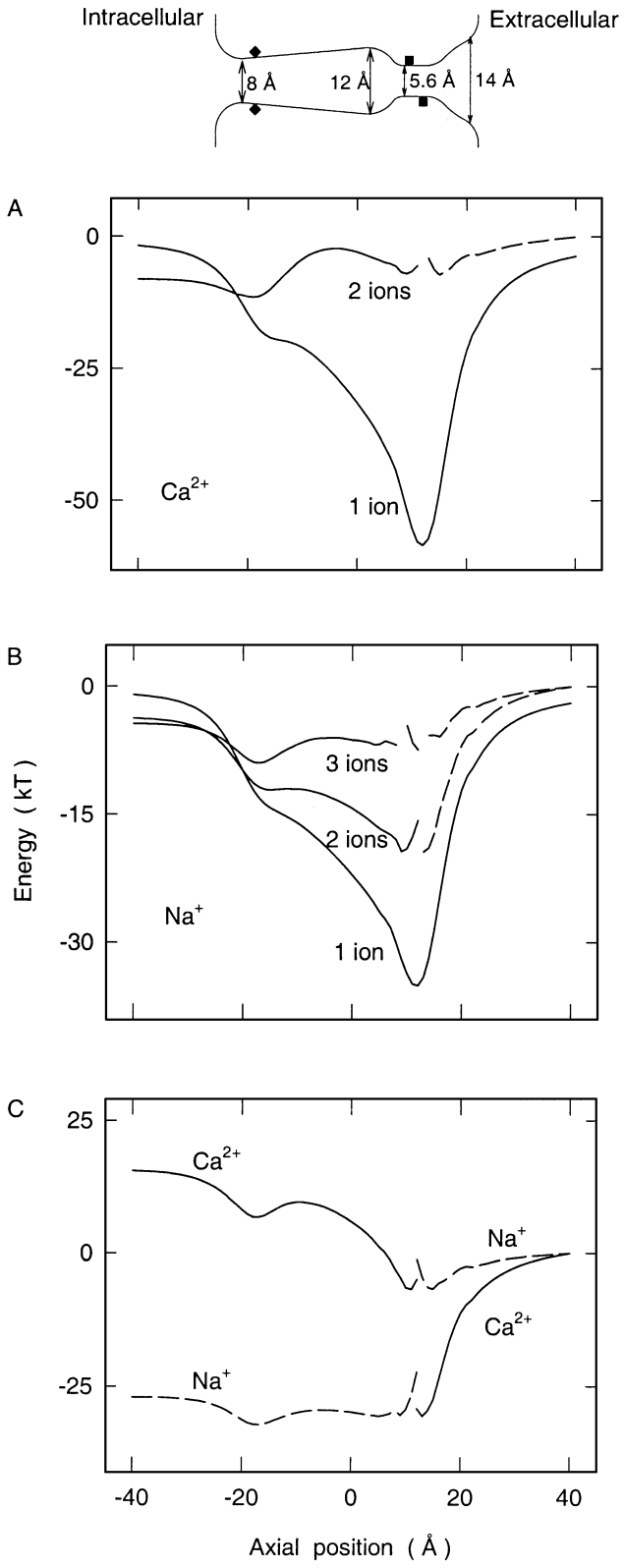

Fig. 5. Shape of a model calcium channel and locations of charge residues (inset). Potential energy profiles of one and two Ca^{2+} ion (A) and one, two and three Na^{+} ions (B), and for the mixed system (C) are shown.

sisting of inner and outer vestibules and a selectivity filter (see the inset in Fig. 5). The selectivity filter is the most important part of the model and requires a careful design in order to reproduce the observed properties of calcium channels. Two critical elements, namely, its size and charges on its walls, are determined from the experimental data. The radius is set to 2.8 Å from the size of tetramethylammonium, the largest permeable ion [109]. The mutation data indicate presence of four negatively charged glutamate residues in the filter region [110]. BD simulations performed with this model has been very successful in replicating many physiological properties of L-type calcium channels. These include current–voltage curves, saturation of conductance with concentration, selectivity against Na^{+} ions, the anomalous mole fraction effect, attenuation of calcium current by external sodium ions, and the effect of mutating glutamate residues on blocking of sodium current [32].

An intuitive understanding of how these properties follow from the ion-channel interactions can be gleaned from a study of the potential energy profiles of ions in the channel. In Fig. 5, we present multi-ion potential profiles for the cases of pure Ca^{2+}, pure Na^{+} and mixed Ca^{2+} and Na^{+} ions in the channel. As shown in (A), a single Ca^{2+} ion is deeply bound (58 kT) in the selectivity filter, and a second Ca^{2+} ion is easily attracted to the channel from the right (extracellular side). The two ions can coexist in the filter region in a semistable equilibrium, until the resident ion on the left climbs over the barrier of 5 kT via thermal fluctuations and exits the channel. Thus, a single Ca^{2+} ion is in a waiting state and entry of a second Ca^{2+} ion triggers a conduction event. Profiles for Na^{+} ions (B) are similar except permeation involves three Na^{+} ions just as in the case of potassium channels. Also, the final barrier to permeation is only 1 kT, which explains why sodium ions conduct much faster. The mechanism of selectivity is explained in diagram (C). When a Na^{+} ion is resident in the filter, a Ca^{2+} ion is attracted to the filter and expels the Na^{+} ion from the channel upon entry. A similar result is obtained when there are two Na^{+} ions in the filter. In the reverse case of a Ca^{2+} ion in the filter, though a Na^{+} ion is still attracted, it is unable to push the Ca^{2+} ion over the large barrier of 16 kT. Thus, once a Ca^{2+} ion enters the channel, Na^{+} ions cannot push it out, and only another Ca^{2+} ion can achieve that feat. This gives a simple explanation of the selectivity mechanism in calcium channels in terms of the electrostatic interactions of ions.

Of the many properties of the calcium channels, the most interesting ones are associated with the blocking effects. In the anomalous mole fraction effect, the channel current vanishes at a certain range of Ca^{2+} concentrations in the presence of a fixed 150 mM Na^{+}, as shown in the inset of Fig. 6A. The BD results (Fig. 6A) indicate that the rapid drop and subsequent vanishing of the channel current is due to the blocking of Na^{+} current by Ca^{2+} ions. Once the Ca^{2+} concentration is high enough to allow two Ca^{2+} ions in the filter, the channel starts conducting again but now Ca^{2+} ions

instead of Na^+. While sodium ions cannot block calcium, their presence in the vestibule can nevertheless slow down entry of a second Ca^{2+} ion necessary for conduction. As illustrated in Fig. 6B, the predicted reduction in the channel current with increasing Na^+ concentration is in excellent agreement with the experimental data. A final example is the effect of mutating one of the glutamate residues to neutral glutamine on the blocking of Na^+ current (Fig. 6C). The mutation leads to a reduction in the depth of the potential well compared to the native case so that entry of a Ca^{2+} ion in the channel is delayed, and the blocking occurs at a higher Ca^{2+} concentration. Trends in the data (inset of C) are again reproduced by the BD simulations.

The level of agreement between theory and experiment obtained from BD studies of calcium channels is substantial and should encourage further applications of the BD method to modeling of other ion channels with limited structural information.

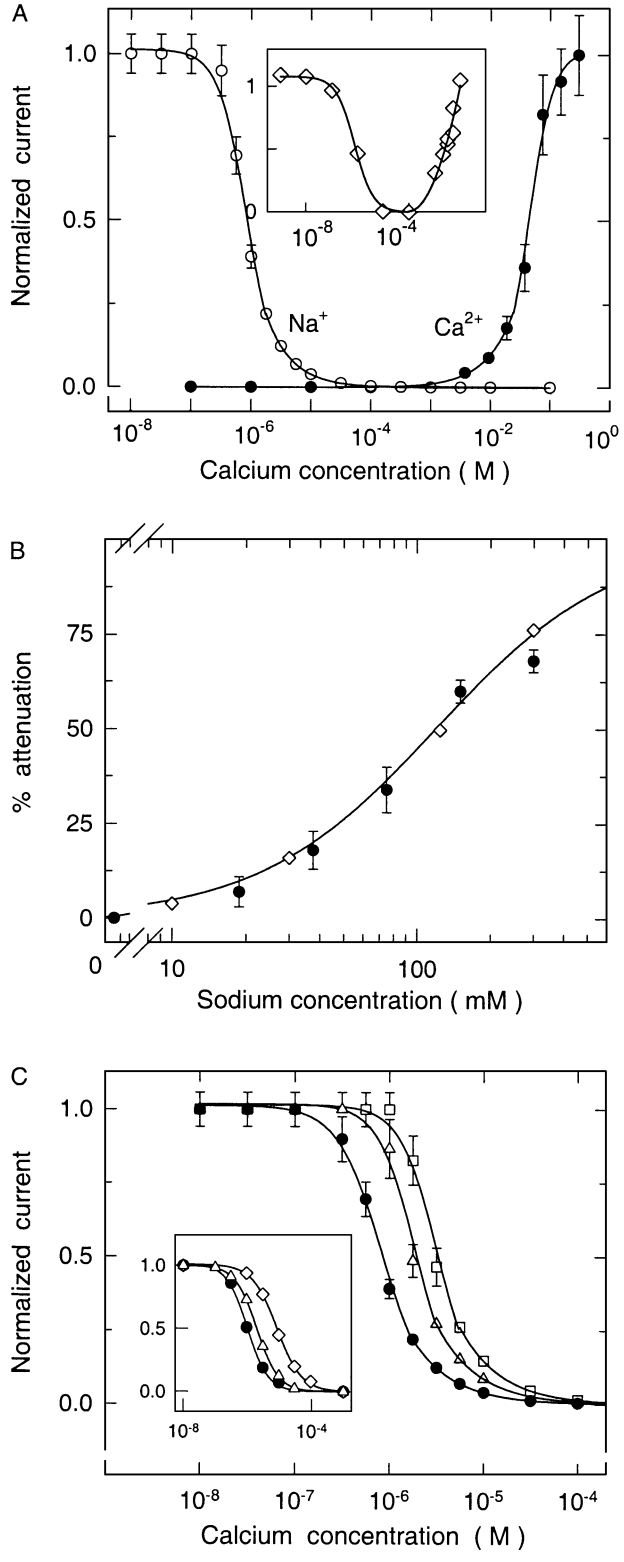

Fig. 6. (A) Mole fraction effect. Ca^{2+} (●) and Na^+ (○) current passing through the channel normalized by the maximum value of each is plotted against the Ca^{2+} concentrations while keeping the Na^+ concentration fixed at 0.15 M. Experimental results [111] are shown in the inset. (B) Attenuation of Ca^{2+} current by Na^+ ions. The percentage reduction in the channel current is plotted against Na^+ concentration while the Ca^{2+} concentration is fixed at 0.15 M (●). The ◇ symbol and dotted line show the experimental data [112]. (C) The effect of removing glutamate charges on channel selectivity. The Na^+ current passing through the channel at different Ca^{2+} concentrations with all four glutamate charges in place (●), the outermost glutamate removed (△) and the innermost glutamate removed (□); otherwise, all conditions are as in (A). Experimental data for wild type (●) and for single glutamate to neutral glutamine mutations of two different residues (△, ◇) are shown in the inset [110]. In all cases, a driving potential of −0.2 V is applied.

4. Conclusions and outlook

In this review, we have attempted to give a flavor of the recent advances in ion channel research brought about by resolution of the structure of channel proteins and progress in computational methods and power. These developments have enabled, for the first time, rigorous study of structure–function relationships in ion channels. Discussion of the merits and shortcomings of various permeation models have led us to identify molecular and Brownian dynamics simulations as the most appropriate tools for this purpose. BD enables calculation of conductance properties while MD can provide input and justification for BD as well as explaining finer details such as size-based selectivity. As practiced, both methods have unjustified approximations and deficiencies that need to be better understood and improved in future work. For example, use of continuum electrostatics in calculation of forces in BD simulations need to be better validated by appealing to MD. Similarly, the force fields employed in MD simulations need to be improved by including the polarization effects, perhaps using ab initio MD as a guide in this process.

Future developments in the field will much depend on the success of the protein chemists in resolving structures of membrane proteins. Because MD simulations rely on atomic-detail structure of a channel, such information is essential for using MD in structure–function studies. On the

other hand, as the success of the BD simulations in explaining the physiological properties of the calcium channel indicates, a detailed tertiary structure is not essential for BD—knowledge of the gross shape of the channel and the approximate locations of the charged residues in the channel wall appear to be sufficient for this purpose. The present difficulties in crystallizing the membrane proteins suggests that BD is likely to play a more prominent role in structure–function studies of ion channels in near future. Therefore, one would like to see more modeling efforts expended in development and applications of the BD method to ion channels.

Acknowledgements

This work is supported by grants from the Australian Research Council and the National Health and Medical Research Council of Australia. We thank our collaborators Toby Allen, Ben Corry, Scott Edwards, Matthew Hoyles, Megan O'Mara and Siu-Cheung Li, who have contributed to the BD and MD studies of channels reported in this review.

References

[1] E. Neher, B. Sakmann, Nature 260 (1976) 799–802.
[2] O.P. Hamill, A. Marty, E. Neher, B. Sakmann, F.J. Sigworth, Pflügers Arch. 391 (1981) 85–100.
[3] D.A. Doyle, J.M. Cabral, R.A. Pfuetzner, A. Kuo, J.M. Gulbis, S.L. Cohen, B.T. Chait, R. MacKinnon, Science 280 (1998) 69–77.
[4] G. Chang, R.H. Spencer, A.T. Lee, M.T. Barclay, D.C. Rees, Science 282 (1998) 2220–2226.
[5] R. Dutzler, E.B. Campbell, M. Cadene, B.T. Chait, R. MacKinnon, Nature 415 (2002) 287–294.
[6] B. Hille, Ionic Channels of Excitable Membranes, 3rd ed., Sinauer Associates, Sunderland, MA, 2001.
[7] R.S. Eisenberg, J. Membr. Biol. 150 (1996) 1–25.
[8] R.S. Eisenberg, J. Membr. Biol. 171 (1999) 1–24.
[9] E.W. McCleskey, J. Gen. Physiol. 113 (1999) 765–772.
[10] W. Nonner, D.P. Chen, B. Eisenberg, J. Gen. Physiol. 113 (1999) 773–782.
[11] C. Miller, J. Gen. Physiol. 113 (1999) 783–787.
[12] D.G. Levitt, J. Gen. Physiol. 113 (1999) 789–794.
[13] K.E. Cooper, E. Jakobsson, P. Wolynes, Prog. Biophys. Mol. Biol. 46 (1985) 51–96.
[14] M.B. Partenskii, P.C. Jordan, Q. Rev. Biophys. 25 (1992) 477–510.
[15] B. Roux, M. Karplus, Annu. Rev. Biophys. Biomol. Struct. 23 (1994) 731–761.
[16] B. Roux, S. Bernèche, W. Im, Biochemistry 39 (2000) 13295–13306.
[17] D.P. Tieleman, P.C. Biggin, G.R. Smith, M.S.P. Sansom, Q. Rev. Biophys. 34 (2001) 473–561.
[18] S. Kuyucak, O.S. Andersen, S.H. Chung, Rep. Prog. Phys. 64 (2001) 1427–1472.
[19] S. Kuyucak, S.H. Chung, Biophys. Chem. 52 (1994) 15–24.
[20] A. Syganow, E. von Kitzing, Biophys. J. 76 (1999) 768–781.
[21] A. Syganow, E. von Kitzing, Eur. Biophys. J. 28 (1999) 393–414.
[22] M.G. Kurnikova, R.D. Coalson, P. Graf, A. Nitzan, Biophys. J. 76 (1999) 642–656.
[23] B. Corry, S. Kuyucak, S.H. Chung, Biophys. J. 78 (2000) 2364–2381.
[24] R.S. Berry, S.A. Rice, J. Ross, Physical Chemistry, 2nd ed., Oxford Univ. Press, New York, 2000.
[25] P. Graf, A. Nitzan, M.G. Kurnikova, R.D. Coalson, J. Phys. Chem., B 104 (2000) 12324–12338.
[26] F. Reif, Fundamentals of Statistical and Thermal Physics, McGraw-Hill, New York, 1965.
[27] E. Jakobsson, S.W. Chiu, Biophys. J. 52 (1987) 33–45.
[28] S. Bek, E. Jakobsson, Biophys. J. 66 (1994) 1028–1038.
[29] S.C. Li, M. Hoyles, S. Kuyucak, S.H. Chung, Biophys. J. 74 (1998) 37–47.
[30] S.H. Chung, M. Hoyles, T.W. Allen, S. Kuyucak, Biophys. J. 75 (1998) 793–809.
[31] S.H. Chung, T.W. Allen, M. Hoyles, S. Kuyucak, Biophys. J. 77 (1999) 2517–2533.
[32] B. Corry, T.W. Allen, S. Kuyucak, S.H. Chung, Biophys. J. 80 (2001) 195–214.
[33] S.H. Chung, T.W. Allen, S. Kuyucak, Biophys. J. 82 (2002) 628–645.
[34] S.H. Chung, T.W. Allen, S. Kuyucak, Biophys. J. 83 (2002) 263–277.
[35] W. Im, S. Seefeld, B. Roux, Biophys. J. 79 (2000) 788–801.
[36] B. Corry, M. Hoyles, T.W. Allen, M. Walker, S. Kuyucak, S.H. Chung, Biophys. J. 82 (2002) 1975–1984.
[37] M.S.P. Sansom, G.R. Smith, C. Adcock, P.C. Biggin, Biophys. J. 73 (1997) 2404–2415.
[38] M.E. Green, J. Lu, J. Phys. Chem., B 101 (1997) 6512–6524.
[39] D.P. Tieleman, H.J.C. Berendsen, Biophys. J. 74 (1998) 2786–2801.
[40] T.W. Allen, S. Kuyucak, S.H. Chung, J. Chem. Phys. 111 (1999) 7985–7999.
[41] S.J. Weiner, P.A. Kollman, D.A. Case, U.C. Singh, C. Ghio, G. Alagona, S. Profeta, P. Weiner, J. Am. Chem. Soc. 106 (1984) 765–784.
[42] B.R. Brooks, R.E. Bruccoleri, B.D. Olafson, D.J. States, S. Swaminathan, M. Karplus, J. Comp. Chem. 4 (1983) 187–217.
[43] J. Hermans, H.J.C. Berendsen, W.F. van Gunsteren, J.P.M. Postma, Biopolymers 23 (1984) 1513–1518.
[44] W.F. van Gunsteren, A.E. Mark, J. Chem. Phys. 108 (1998) 6109–6116.
[45] M.P. Allen, D.J. Tildesley, Computer Simulation of Liquids, Oxford Univ. Press, London, 1987.
[46] D. Frenkel, B. Smit, Understanding Molecular Simulation: From Algorithms to Applications, Academic Press, San Diego, 1996.
[47] D.C. Rapaport, The Art of Molecular Dynamics Simulation, Cambridge Univ. Press, Cambridge, 1995.
[48] W. Wang, O. Donini, C.M. Reyes, P.A. Kollman, Annu. Rev. Biophys. Biomol. Struct. 30 (2001) 211–243.
[49] H.J.C. Berendsen, J.P.M. Postma, W.F. van Gunsteren, J. Hermans, in: B. Pullman (Ed.), Intermolecular Forces, Reidel, Dordrecht, 1981, pp. 331–342.
[50] W.L. Jorgensen, J. Chandrasekhar, J.D. Madura, R.W. Impey, M.L. Klein, J. Chem. Phys. 79 (1983) 926–935.
[51] F. London, Z. Phys. 63 (1930) 245.
[52] A. Wallqvist, R.D. Mountain, Rev. Comput. Chem. 13 (1999) 183–247.
[53] C. Sagui, T.A. Darden, Annu. Rev. Biophys. Biomol. Struct. 28 (1999) 155–179.
[54] P.P. Ewald, Ann. Phys. 64 (1921) 253–287.
[55] A. Suenaga, Y. Komeiji, M. Uebayasi, T. Meguro, M. Saito, I. Yamato, Biosci. Rep. 18 (1998) 39–48.
[56] P.S. Crozier, D. Henderson, R.L. Rowley, D.D. Busath, Biophys. J. 81 (2001) 3077–3089.
[57] E. Guàrdia, R. Rey, J.A. Padró, Chem. Phys. 155 (1991) 187–195.
[58] D.E. Smith, L.X. Dang, J. Chem. Phys. 100 (1994) 3757–3766.
[59] G.M. Torrie, J.P. Valleau, J. Comp. Phys. 23 (1977) 187–199.
[60] T. Woolf, B. Roux, Biophys. J. 72 (1997) 1930–1945.
[61] D.P. Tieleman, S.J. Marrink, H.J.C. Berendsen, Biochim. Biophys. Acta 1331 (1997) 235–270.

[62] P. Jordan, Biophys. J. 58 (1990) 1133–1156.
[63] B. Roux, M. Karplus, J. Am. Chem. Soc. 115 (1993) 3250–3262.
[64] W. Kohn, Rev. Mod. Phys. 71 (1999) 1253–1266.
[65] R. Car, M. Parrinello, Phys. Rev. Lett. 55 (1985) 2471–2474.
[66] J.H. Morais-Cabral, Y. Zhou, R. MacKinnon, Nature 414 (2001) 37–42.
[67] Y. Zhou, J.H. Morais-Cabral, A. Kaufman, R. MacKinnon, Nature 414 (2001) 43–48.
[68] L.G. Cuello, J.G. Romero, D.M. Cortes, E. Perozo, Biochemistry 37 (1998) 3229–3236.
[69] L. Heginbotham, M. LeMasurier, L. Kolmakova-Partensky, C. Miller, J. Gen. Physiol. 114 (1999) 551–559.
[70] A. Gross, L. Columbus, K. Hideg, C. Altenbach, W.L. Hubbell, Biochemistry 38 (1999) 10324–10335.
[71] E. Perozo, D.M. Cortes, L.G. Cuello, Science 285 (1999) 73–78.
[72] Y.S. Liu, P. Sompornpisut, E. Perozo, Nat. Struct. Biol. 8 (2001) 883–887.
[73] S. Berneche, B. Roux, Biophys. J. 78 (2000) 2900–2917.
[74] S. Berneche, B. Roux, Nature 414 (2001) 73–77.
[75] I.H. Shrivastava, M.S.P. Sansom, Biophys. J. 78 (2000) 557–570.
[76] L. Guidoni, V. Torre, P. Carloni, Biochemistry 38 (1999) 8599–8604.
[77] L. Guidoni, V. Torre, P. Carloni, FEBS Lett. 477 (2000) 37–42.
[78] J. Åqvist, V. Luzhkov, Nature 404 (2000) 881–884.
[79] V.B. Luzhkov, J. Åqvist, Biochim. Biophys. Acta 1481 (2000) 360–370.
[80] V.B. Luzhkov, J. Åqvist, Biochim. Biophys. Acta 1548 (2001) 194–202.
[81] T.W. Allen, S. Kuyucak, S.H. Chung, Biophys. J. 77 (1999) 2502–2516.
[82] T.W. Allen, A. Bliznyuk, A.P. Rendell, S. Kuyucak, S.H. Chung, J. Chem. Phys. 112 (2000) 8191–8204.
[83] P.C. Biggin, G.R. Smith, I. Shrivastava, S. Choe, M.S.P. Sansom, Biochim. Biophys. Acta 1510 (2001) 1–9.
[84] K.M. Ranatunga, I.H. Shrivastava, G.R. Smith, M.S.P. Sansom, Biophys. J. 80 (2001) 1210–1219.
[85] T.W. Allen, S. Kuyucak, S.H. Chung, Biophys. Chem. 86 (2000) 1–14.
[86] R.J. Mashl, Y. Tang, J. Schnitzer, E. Jakobsson, Biophys. J. 81 (2001) 2473–2483.
[87] A. Burykin, C.N. Schutz, J. Villa, A. Warshel, Proteins 47 (2002) 265–280.
[88] M. LeMasurier, L. Heginbotham, C. Miller, J. Gen. Physiol. 118 (2001) 303–313.
[89] D. Meuser, H. Splitt, R. Wagner, H. Schrempf, FEBS Lett. 462 (1999) 447–452.
[90] H. Schrempf, O. Schmidt, R. Kümmerlen, S. Hinnah, D. Müller, M. Betzler, T. Steinkamp, R. Wagner, EMBO J. 14 (1995) 5170–5178.
[91] J.L. Rae, R.A. Levis, R.S. Eisenberg, Ionic channels in ocular epithelia, in: T. Narahashi (Ed.), Ion Channels, vol. 1, Plenum, New York, 1988, pp. 283–327.
[92] R. Coronado, R.L. Rosenberg, C. Miller, J. Gen. Physiol. 76 (1980) 425–446.
[93] L. Heginbotham, T. Abramson, R. MacKinnon, Science 258 (1992) 1152–1155.
[94] R. MacKinnon, S.L. Cohen, A. Kuo, A. Lee, B.T. Chait, Nature 280 (1998) 106–109.
[95] Z. Lu, A.M. Klem, Y. Ramu, Nature 413 (2001) 809–813.
[96] I.H. Shrivastava, C.E. Capener, L.R. Forrest, M.S.P. Sansom, Biophys. J. 78 (2000) 79–92.
[97] C.E. Capener, I.H. Shrivastava, K.M. Ranatunga, L.R. Forrest, G.R. Smith, M.S.P. Sansom, Biophys. J. 78 (2000) 2929–2942.
[98] G.A. Thompson, M.L. Leyland, I. Ashmole, M.J. Sutcliffe, P.R. Stanfield, J. Physiol. 526 (2000) 231–240.
[99] Y. Kubo, Y. Murata, J. Physiol. 531 (2001) 645–660.
[100] D.W. Urry, Proc. Natl. Acad. Sci. U. S. A. 68 (1971) 672–676.
[101] O.S. Andersen, R.E. Koeppe, Physiol. Rev. 72 (1992) 89–158.
[102] B. Roux, Acc. Chem. Res. 35 (2002) 366–375.
[103] S. Edwards, B. Corry, S. Kuyucak, S.H. Chung, Biophys. J. 83 (2002) 1348–1360.
[104] M. Sancho, M.B. Partenskii, V. Dorman, P.C. Jordan, Biophys. J. 68 (1995) 427–433.
[105] B. Roux, B. Prodhom, M. Karplus, Biophys. J. 68 (1995) 876–892.
[106] F. Tian, K.C. Lee, W. Hu, T.A. Cross, Biochemistry 35 (1996) 11959–11966.
[107] F. Tian, T.A. Cross, J. Mol. Biol. 285 (1999) 1993–2003.
[108] R.W. Tsien, P. Hess, E.W. McCleskey, R.L. Rosenberg, Annu. Rev. Biophys. Chem. 16 (1987) 265–290.
[109] E.W. McCleskey, W. Almers, Proc. Natl. Acad. Sci. U. S. A. 82 1985, pp. 7149–7153.
[110] J. Yang, P.T. Ellinor, W.A. Sather, J.F. Zhang, R.W. Tsien, Nature 366 (1993) 158–161.
[111] W. Almers, E.W. McCleskey, P.T. Palade, J. Physiol. 353 (1984) 565–583.
[112] L. Polo-Parada, S.J. Korn, J. Gen. Physiol. 109 (1997) 693–702.